2-24-2019

Magnetic Field Aided Indoor Navigation

William F. Storms

Magnetic Field Aided Indoor Navigation

THESIS

William F. Storms, Captain, USAF

AFIT/GE/ENG/09-44

DEPARTMENT OF THE AIR FORCE
AIR UNIVERSITY

AIR FORCE INSTITUTE OF TECHNOLOGY

Wright-Patterson Air Force Base, Ohio

The views expressed in this thesis are those of the author and do not reflect the official policy or position of the United States Air Force, Department of Defense, or the United States Government.

AFIT/GE/ENG/09-44

Magnetic Field Aided Indoor Navigation

THESIS

Presented to the Faculty

Department of Electrical and Computer Engineering

Graduate School of Engineering and Management

Air Force Institute of Technology

Air University

Air Education and Training Command

In Partial Fulfillment of the Requirements for the

Degree of Master of Science in Electrical Engineering

William F. Storms, B.S.E.E.

Captain, USAF

March 2009

AFIT/GE/ENG/09-44

Magnetic Field Aided Indoor Navigation

William F. Storms, B.S.E.E.
Captain, USAF

Approved:

/signed/	24 Feb 2009
Dr. J.F. Raquet (Chairman)	date
/signed/	24 Feb 2009
Lt Col M.J. Veth (Member)	date
/signed/	24 Feb 2009
Dr. M.J. Havrilla (Member)	date

AFIT/GE/ENG/09-44

Abstract

This research effort examines inertial navigation system aiding using magnetic field intensity data and a Kalman filter in an indoor environment. Many current aiding methods do not work well in an indoor environment, like aiding using the Global Positioning System. The method presented in this research uses magnetic field intensity data from a three-axis magnetometer in order to estimate position using a maximum – likelihood approach. The position measurements are then combined with a motion model using a Kalman filter. The magnetic field navigation algorithm is tested using a combination of simulated and real measurements. These tests are conducted using a magnetic field intensity map of the entire test environment. The result of these tests show that the position aiding algorithm is capable of generating positon estimates from real data within less than 1 meter of the true trajectory, with most estimates .3 meters away from the true trajectory in a laboratory hallway environment. To further explore the capabilities of the position aiding algorithm, a leader-follower scenario is implemented. In this scenario, the follower uses magnetic field intensity data collected by the leader to estimate its current position and attempt to follow the leader's trajectory. The results show that tracking is possible, and that the measurement span of the leader has a large impact on the result.

Acknowledgements

I would like to thank my Lord and Savior, Jesus Christ, for the many blessings in my life, of which AFIT is one. I would like to thank my wonderful wife who supported me throughout this process, without your support I don't know if I would have remained as sane as I have. I would also like to thank Dr. Raquet for being there to provide guidance and that extra push to make me think a little harder and do a little more work, even when I thought I was done and had done it all. Finally, I would like to thank all of my instructors for their willingness to share their knowledge, time, and expertise. Thank you.

William F. Storms

Table of Contents

Page

Abstract iv

Acknowledgements v

Table of Contents vi

List of Figures viii

List of Tables x

I. Introduction 1
1.1 Modes of Operation 2
1.2 Thesis Overview 2

II. Background 4
2.1 Coordinate Transformations 4
2.2 Strapdown Inertial Navigation Systems 5
2.2.1 Accelerometers 6
2.2.2 Gyroscopes 7
2.2.3 Inertial Navigation System Aiding 8
2.3 Aiding Techniques 9
2.3.1 Kalman Filtering 9
2.3.2 Magnetic Field Based Navigation 13
2.4 Summary 21

III. Methodology 22
3.1 Required Equipment 22
3.1.1 Three-Axis Magnetometers 23
3.1.2 Laptop 23
3.2 Magnetic Field Intensity Map 24
3.2.1 Magnetic Map Data Collection 24
3.2.2 Magnetic Map Data Processing 26
3.3 System Model 27
3.4 Magnetic Aided Position Algorithm 29
3.4.1 Propagation Equations 30
3.4.2 Measurement Generation 30
3.4.3 Measurement Update Equations 33
3.5 Leader-Follower Methodology 34

Page

3.5.1 Map Generation 34
3.5.2 Follower Vehicle Control 34
3.6 Summary 37

IV. Implementation 39
4.1 Magnetic Field Intensity Variations By Location 39
4.2 Magnetic Field Intensity Map 40
4.2.1 Main Hallway Magnetic Field Intensity Map . . 41
4.2.2 Side Hallway Magnetic Field Intensity Map . . . 42
4.3 Magnetic Aided Position Algorithm Results 43
4.3.1 Example Discrete Bivariate Gaussian PDF . . . 45
4.3.2 Example Likelihood Function Result 45
4.3.3 Example Bayes' Rule Implementation Example 45
4.4 Magnetic Field Aided Trajectory Estimation 47
4.4.1 Generated Trajectory Simulation 48
4.4.2 Real Trajectory and Measurements 53
4.5 Leader-Follower Algorithm Implementation 56
4.5.1 Leader-Follower Performance Analysis 57
4.5.2 Leader-Follower Estimation Error 60
4.6 Summary 64

V. Conclusions and Recommendations 67
5.1 The Magnetic Aided Position Algorithm 67
5.2 Magnetic Aided Position Algorithm Tests 67
5.3 The Way Ahead 69

Appendix A. Leader-Follower Coordinate Transformation 71

Bibliography 73

List of Figures

Figure		Page
2.1.	Inertial Navigation System Performance Comparison	9
2.2.	Earth's Main Dipole Magnetic Field	15
2.3.	Map of Magnetic Fingerprints	19
3.1.	Photo of the Honeywell HMR2300®	24
3.2.	Layout of Test Environment	25
3.3.	Relationship Between the Navigation and Body Reference Frame	26
3.4.	Photo of Data Collection Vehicle	27
3.5.	PID Controller Block Diagram	36
3.6.	Step Response of PID Controller without Process Noise	37
3.7.	Step Response of PID Controller with Process Noise	38
4.1.	Hallway Relationships for Magnetic Field Intensity Comparison	40
4.2.	Magnetic Field Intensity Comparison	41
4.3.	Example Two-Dimensional Magnetic Map	42
4.4.	Main Hallway Magnetic Intensity Maps	43
4.5.	Zoomed in View of Main Hallway Magnetic Intensity Maps	43
4.6.	Side Hallway Magnetic Intensity Maps	44
4.7.	Zoomed in View of Side Hallway Magnetic Intensity Maps	44
4.8.	Example Discrete Probability Density Function	46
4.9.	Example Discrete Likelihood Function Result	46
4.10.	Example Discrete Post-Measurement Probability Density Function	47
4.11.	Example Simulated Trajectory	50
4.12.	Filter RMS Values – No Turn Command	51
4.13.	Filter RMS Values – Turn Command	52
4.14.	Ensemble Statistics – No Turn Command	53

Figure Page

4.15. Ensemble Statistics – Turn Command 54

4.16. Real Trajectory Near Center of Hallway 55

4.17. Position Error Plots – First Non-Simulated Trajectory 56

4.18. Measurement Residuals of First Non-Simulated Trajectory . . . 57

4.19. Real Trajectory Near Right Side of Hallway 58

4.20. Position Error Plots – Second Non-Simulated Trajectory 59

4.21. Measurement Residuals of Second Non-Simulated Trajectory . 60

4.22. Position Error Plots – First Non-Simulated Trajectory with Corrected System Model 62

4.23. Position Error Plots – Second Non-Simulated Trajectory with Corrected System Model 63

4.24. Example Failure Mode Induced by Small Magnetic Variations . 64

4.25. Follower's Trajectory With Respect to Leader's Reference Frames – Right Veering Leader 65

4.26. Follower's Trajectory With Respect to Leader's Reference Frames – Left Veering Leader 65

4.27. Cross-Track Errors Between the Follower and the Leader – With Position Reset 66

4.28. Cross-Track Errors Between the Follower and the Leader – Without Position Reset 66

A.1. Geometric Representation of Lead-Follow Reference Transformation 72

List of Tables

Table		Page
2.1.	General Accelerometer and Gyroscope Errors	6
2.2.	IMU Performance Parameters	10
3.1.	Example of Measured Magnetic Fields	28
3.2.	Example Map Data Structure	28
4.1.	Simulation Parameter Values	61
4.2.	Leader-Follower Performance Comparison	61

I. Introduction

Precision navigation has become an important aspect of military and commercial applications. The advent of Global Navigation Satellite Systems (GNSS) has provided an unprecedented level of accuracy to a wide variety of users. Once these users experience a specific level of accuracy, they become dependant on that level of accuracy and desire more accuracy in more situations. The position solutions provided by GNSS have provided sub-meter level accuracy in many applications, but the positioning solutions from these types of navigational aids are only available when the receiver has uninterrupted access to at least four satellites [9]. While overall satellite coverage of the Earth has increased, environments such as urban canyons and inside buildings can prevent the acquisition of the required satellite signals. Without adequate satellite coverage, the sub-meter level positioning solutions cannot be obtained. At the same time, there is an increasing desire to develop autonomous, miniature vehicles. The navigation of these systems is generally completed with inertial navigation systems aided by GNSS position solutions. If the GNSS position solutions are not available, these miniature vehicles will not be able to navigate with the required level of accuracy. This research will investigate the feasibility of using magnetic fields to aid an inertial system when GNSS signals are not available.

The research presented here examines the uniqueness of magnetic field variations from one location to the next in an indoor environment. Using this uniqueness, the feasibility of using magnetic field variations to accurately estimate the trajectory of a vehicle is presented. Finally, the magnetic aided position algorithm developed to estimate a vehicle's trajectory is applied to a trajectory tracking implementation. The following research examines the spatial variations of magnetic field intensities, but does not include an in-depth analysis of the variations with respect to time.

The use of magnetic field variations to aid outdoor navigation has been suggested by various authors [3, 16] and successfully implemented by Wilson, Kline-Schoder, Kenton, Sorensen, and Clavier [19]. The methods proposed, and used, implement a terrain navigation algorithm, where the terrain map is replaced by a map of magnetic field intensities, to determine the position based on the measured magnetic field intensity. The approach presented in this research is based on a multiple beam terrain navigation approach originally developed for submarine navigation [11]. However, the algorithm has been adapted to use a magnetic field intensity map instead of a terrain map and three-axis magnetometers instead of a depth/terrain height measuring device.

1.1 Modes of Operation

The magnetic aided position algorithm is implemented using two different approaches. The first approach estimates a vehicle's trajectory using a magnetic field intensity map of the entire area to be traversed, which provides a position solution relative to the area that is included in the map. The second method uses magnetic field intensity data collected by a lead vehicle, or the leader. The leader then passes this information to a second vehicle, the follower, that uses the magnetic data, combined with the position estimate of the leader, to estimate its position relative to the leader.

1.2 Thesis Overview

Chapter II begins with a brief overview of the components used in an inertial navigation system (INS) and the types of errors associated with these devices. A performance analysis of three different grades of INS is shown to demonstrate the need for position aiding. The performance analysis is followed by a brief description of the Earth's magnetic fields and the sources of variations of the main field. The history of using magnetic fields to aid in navigation is then covered, to include animals that find there way around the Earth using magnetic fields. The final section of Chapter II

introduces and explains the multiple beam terrain navigation approach that was the starting point for this research.

The third chapter of this thesis covers the methods used in the design of the magnetic aided position algorithm. The chapter begins by detailing the equipment used and required for implementation of this aiding algorithm. The next section in Chapter III describes the magnetic field intensity map generation process. This section includes information on map grid point spacing, as well as the layout and orientation of the test environment. Once the map generation has been covered, the system model used in this research is defined and the magnetic aided position algorithm, as implemented, is explained. The final piece of Chapter III is the leader-follower algorithm. This section explains the different method used for map generation, as well as the design of the tracking controller used on the follower to aid in tracking the estimated trajectory of the leader.

Chapter IV presents the results generated using the methods presented in Chapter III. The chapter begins by showing the result of the map generation process. Following the map generation, the ensemble statistics from 100 Monte Carlo (MC) runs are presented and compared with the filter estimates to show the accuracy of the system model implemented in the Kalman filter. In addition to the MC results, the position errors associated with using real measurements are shown and explained. The final set of results show the performance of the leader-follower algorithm. The leader-follower algorithm magnified some underlying problems with the magnetic aiding position algorithm. These problems are explained and some options for minimizing their effects are described, implemented, and the results are presented.

The thesis closes with a summary of the information presented in the preceding sections and chapters. Chapter V closes with a list of recommendations that will improve the results and make the magnetic aided position algorithm more robust.

II. Background

NAVIGATION on the Earth requires a few key elements. The first is a reference frame and the ability to move between different frames using coordinate transformations. The coordinate transformation relies on the angular relationship between reference frames to rotate one frame onto another. The coordinate transformations and positioning information are obtained using information provided by gyroscopes and accelerometers. In order to properly understand the research presented in this document, the concepts of coordinate transformations and reference frames must be understood. Following a brief description of coordinate transformations and reference frames, the relationship between accelerometers, gyroscopes, and coordinate transformation is defined.

As part of this relationship definition, the errors common to accelerometers and gyroscopes are presented. Due to the errors inherent in these inertial sensors, inertial navigation systems, must be aided. While numerous aiding techniques are available, the Kalman filter method is used throughout this research and is explained in this chapter. The Kalman filter aiding method can be successfully used to aid inertial systems with many different types of position measuring devices. This chapter will conclude with a look at some emerging techniques that use the Earth's magnetic field to aid navigation systems.

2.1 Coordinate Transformations

Navigation on the earth uses numerous reference frames. A reference frame is defined by Titterton and Weston as "the set of axes to which the measurements and estimated quantities generated within an inertial system are referenced" [16]. There are many resources that can be used to define these reference frames [17]. In addition to being able to understand how each reference frame relates to the earth, it is also important to understand how these frames relate to each other. While "the concept of *navigation reference frames* is an important fundamental for expressing the position, velocity, and orientation of a body" [17], coordinate transformations are the tools

used to make this information mean something. Without the ability to move from one reference frame to another, vehicles in different reference frames would not be able to determine their position in relation to each other.

The Direction Cosine Matrix (DCM) is one way of rotating between reference frames. The DCM uses geometry and vector math to relate the two reference frames. The DCM uses "the inner product of each unit basis vector in one frame with each unit basis vector in another frame" [17]. The standard notation for the DCM is C_a^b, where a is the reference frame that is being converted from and b is the reference frame being converted to. The angles used to determine the DCM are provided by gyroscopes in the navigation system. A vector expressed in frame a (x^a) can be rotated into frame b (x^b) using

$$x^b = C_a^b x^a \tag{2.1}$$

2.2 Strapdown Inertial Navigation Systems

Strapdown inertial navigation systems (SINS) are used to determine a vehicle's position on or over the Earth by determining the vehicle's attitude and motion. There are many different ways to make a strapdown navigation system, but they all contain the same major components. The differences between SINS are driven by the application of that particular SINS. The main factor in determining what a particular SINS will look like is the accuracy requirement for that particular application. The accuracy of a SINS is generally expressed as a rate by which the SINS deviates from the actual position (i.e. x meters per sec/min/hour). For the purposes of this research, the components that make up a SINS will be broken down into two main categories: accelerometers and gyroscopes. Each of these components are necessary for the vehicle to calculate its attitude and position with respect to the earth. The overall accuracy of the SINS comes from the accuracy of these two components. The sources of error for each of these devices will be discussed in their respective sections.

2.2.1 Accelerometers. Accelerometers measure the acceleration of an object [2]. The vehicle's position can be found by integrating the acceleration twice. Fraden states that this becomes an important truth when dealing with applications that are in a "noisy environment" (this means an environment that has some sort of condition that would make the sensor believe it is accelerating in a direction that the aircraft is not actually moving in, i.e., vibrations). This is important because in order to calculate velocity and acceleration from position, it is necessary to take the first and second derivative of the position, respectively. Taking the derivative of a "noisy" signal increases the level of noise in the signal to the point of making it unusable or highly inaccurate [2]. Since accelerometers measure acceleration, there is no need to take the derivative, just the integral, which handles "noisy" signals well.

Titterton and Weston go into the mechanics and the theory behind accelerometers in depth. For this research, only a top-level description is needed. Accelerometers will measure acceleration generated from the force exerted by the aircraft to which it is mounted as well as the force of gravity. Therefore, the output of the accelerometer must have the gravitational acceleration acting on it subtracted out at any given time [16].

As stated in Section 2.2, there are various sources of error within accelerometers that will diminish the overall performance of a SINS. A full description of these are located in Titterton and Weston. A brief description is given in Table 2.1.

Table 2.1: General Accelerometer and Gyroscope Errors [16]

Type of Error	Error Description
Fixed Bias	Displacement from zero "when the applied acceleration is zero"
Scale-Factor Errors	Non-exact "ratio of change in the output signal to a change in the input acceleration"
Alignment Errors	Sensor axes is non-orthogonal due to "manufacturing imperfections"

Accelerometers provide the linear accelerations needed to calculate how the vehicle is moving in the inertial frame with respect to the body frame. Generally, there is one accelerometer oriented in each of the three Cartesian axes, (x, y, z). This information is needed in the navigation frame of reference to be of use. As mentioned in Section 2.1, a coordinate transformation will be used to get this data into the correct reference frame. Gyroscopes provide the angular orientation needed to generate this coordinate transformation.

2.2.2 Gyroscopes. While accelerometers use Newton's Second Law of Motion to calculate the acceleration of the aircraft [16], the gyroscope (called "gyro" for short) measures the rotation of the aircraft's body [2].

Mechanical gyros are the foundation for all other types of gyros. For a listing of the different types, see [2] and [16]. SINS generally use micro-machined electromechanical systems (MEMS) gyros or optical gyros [16]. This paper will only cover the basic operation of a mechanical gyro because the optical and MEMS gyros were developed using the basic principles of mechanical gyros. The typical two-degrees-of-freedom mechanical gyro is made up of a spinning wheel (called the rotor), an inner and outer gimbal, and angle pick-off sensors. When the rotor is spinning, "it defines a direction in space that remains fixed in the inertial reference frame" [16]. By having this fixed frame of reference, rotation can be detected. Titterton and Weston give a very in-depth look at the physics behind this phenomenon. To paraphrase their description, the gimbals of the gyro are fixed to the aircraft and move with the body reference frame, with the rotor suspended along the spin axis inside the gimbals, it is able to maintain its direction of rotation and stays true to the inertial reference frame. The "orientation of the case (gimbals) of the instrument with respect to the direction of the spin axis" [16] can be measured and then used in the coordinate transformation to find out the attitude of the aircraft in the navigation frame. A typical SINS will have three gyros, one to measure the roll rate, one to measure the pitch rate, and one

to measure the yaw rate. These rates are then used to determine the attitude of the aircraft.

Just like with accelerometers, there are errors associated with gyros and they can be viewed in Table 2.1.

Once the angle rates have been measured, this information, along with the measured accelerations along each axis, will be passed to on-board computers to calculate the actual position of the aircraft. The accelerometers and gyroscopes are packaged together in an inertial measurement unit (IMU). Once the on-board computer system is added, the total system is called an inertial navigation system (INS).

2.2.3 Inertial Navigation System Aiding. Inertial navigation systems need to be aided when used over extended periods of time. The definition of extended, in this case, is based on the grade of INS being used and the application. Table 2.2 shows the magnitudes of the INS errors associated with three grades of inertial systems: Navigation (H764-Q), Tactical (HG-1700), and Commercial (Crista IMU).

Figure 2.1 shows the difference in uncertainty as a function of time for each grade, using the parameters listed in Table 2.2. From this figure, it is clear that a Commercial grade INS would not be sufficient if the application required a solution within 1 deg of latitude after 30 minutes of travel. Instead, the navigation grade INS would be necessary to achieve this level of accuracy.

Navigation grade inertial systems are larger in size and more expensive than tactical and commercial grade inertial systems. For systems that are expendable, such as missiles, bombs, micro-air vehicles (MAVs), etc., the cheaper the system the better. However, these systems require a high level of accuracy to be effective. These realities have led to many different aiding techniques to assist the inertial systems with their navigation solutions.

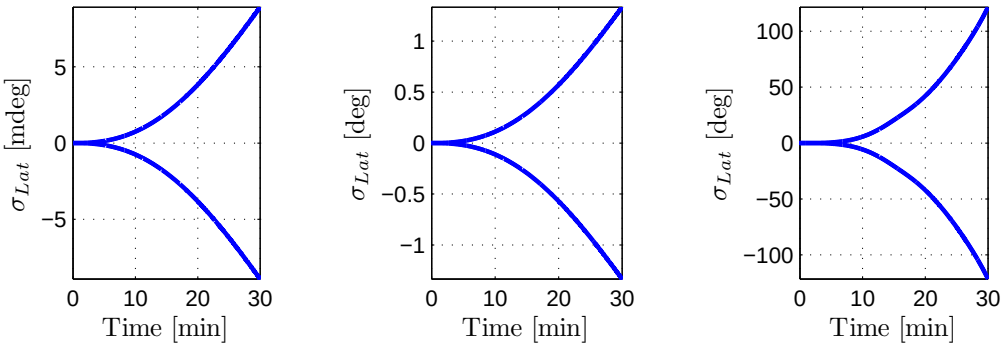

(a) Navigation Grade (b) Tactical Grade (c) Commercial Grade

Figure 2.1: Inertial navigation system performance comparison. (a) The latitude uncertainty of a typical navigation-grade INS over a 30 minute period. (b) The latitude uncertainty of a typical tactical-grade INS over a 30 minute period. (c) The latitude uncertainty of a typical commercial-grade INS over a 30 minute period.

2.3 Aiding Techniques

Kalman filtering has proven to be an effective algorithm when using aiding measurements with an INS [16]. Many navigation measurement systems are available to aid the INS. Some of these techniques use sensors on-board the vehicle, such as Doppler radar, altimeters, magnetic measurements, terrain-referenced navigation, scene matching, and continuous visual navigation [16]. Other techniques are external to the vehicle, such as radio navigation aids, satellites, star trackers, or ground-based radar trackers [16]. For the purposes of this research, INS-aiding via magnetic measurements will be discussed.

2.3.1 Kalman Filtering. A Kalman filter (KF) is "an optimal recursive data processing algorithm" [8] that is used to generate an estimate of the states based on current measurement values and all previous measurements. However, the KF does not require specific knowledge of previous measurements. Instead, the KF uses the information stored in the previous estimate and covariance associated with this estimate to account for this prior information. There are three basic assumptions that must be met in order for the KF to be the optimal estimator.

Table 2.2: IMU Performance Parameters from [18]

Parameters (units)	Crista IMU	HG-1700	H764-G
Sampling interval (ms)	5.0	10.0	3.906
Gyro bias sigma (deg $/hr$)	1800	1.0	0.0015
Gyro bias time constant (hr)	1	1	1
Angular random walk (deg $/\sqrt{hr}$)	2.23	0.3	0.002
Gyro scalefactor sigma (PPM)	10000	150	5
Accel bias sigma (m/s^2)	0.196	0.0098	2.45×10^{-4}
Accel bias time constant (hr)	1	1	1
Velocity random walk ($m/s/\sqrt{hr}$)	0.261	0.57	0.0143
Accel scalefactor sigma (PPM)	10000	300	100

These assumptions are that the system dynamics can be modeled as a linear system and that measurement noises are both white and Gaussian [8]. With these assumptions in mind, the system model used in a KF is comprised of a dynamics matrix, $\mathbf{F}$, a matrix that captures the intensities of the noises driving the system model, $\mathbf{Q}$, and a matrix that describes how control inputs affect the outcome of the system, $\mathbf{B}$. These matrices satisfy the stochastic differential equation

$$\dot{\mathbf{x}}(t) = \mathbf{F}(t)\mathbf{x}(t) + \mathbf{B}(t)\mathbf{u}(t) + \mathbf{G}(t)\mathbf{w}(t) \tag{2.2}$$

where $\mathbf{w}(t)$ represents the white, Gaussian, driving noises on the system [8]. The matrix $\mathbf{Q}$ is defined as $E\left\{\mathbf{w}(t)\mathbf{w}(t)^T\right\} = \mathbf{Q}\delta(t)$. In real-life applications, measurements are generally available at discrete points in time. Therefore, in order to combine the state estimate with the measurements, Equation 2.2 must be discretized, which results in a stochastic difference equation. The equivalent stochastic difference equation for Equation 2.2 which is developed in [8], becomes,

$$\mathbf{x}(t_{k+1}) = \mathbf{\Phi}(t_{k+1}, t_k)\mathbf{x}(t_k) + \mathbf{B_d}(t_k)\mathbf{u}(t_k) + \mathbf{w}_d(t_k) \tag{2.3}$$

where

$$\begin{aligned}
\Delta t &= t_{k+1} - t_k \\
\mathbf{\Phi}(t_{k+1}, t_k) &= e^{\mathbf{F}(t_k)\Delta t} \\
B_d &= \int_{t_k}^{t_{k+1}} \mathbf{\Phi}(t_{k+1}, \tau)\mathbf{B}(\tau)d\tau \\
E[\mathbf{w_d}(t_k)\mathbf{w_d}^T(t_k)] &= \int_{t_k}^{t_{k+1}} \mathbf{\Phi}(t_{k+1}, \tau)\mathbf{G}(\tau)\mathbf{Q}(\tau)\mathbf{G}^T(\tau)\mathbf{\Phi}^T(t_{k+1}, \tau)d\tau.
\end{aligned} \tag{2.4}$$

2.3.1.1 Propagation and Measurement Updates. Using the system model as defined above, the first step in the Kalman filtering process is to propagate the current information forward in time. This step is a prediction of how the states will change over a specific time interval, Δt. For example, if a vehicle moves forward from an initial position, $\mathbf{x}_0$, at a constant velocity of 60 mph for 10 minutes (Δt), the vehicle will be exactly 10 miles ahead of its initial position, if the system model is perfect and there are no other error sources associated with the vehicle. The system dynamics matrix, $\mathbf{F}$, contains the behavior information of the system, in the case of the example, it would reflect a constant velocity. The actual velocity of 60 mph would be provided in the initial condition for the system. The KF advances the state estimates based on the system model, but then estimates the uncertainty of that state estimate by adding the white, Gaussian noises. This is done by applying $\hat{\mathbf{x}}(t_k^+) = \mathbf{x_0}$ and $\mathbf{P}(t_k^+) = \mathbf{P_0}$ to

$$\hat{\mathbf{x}}(t_{k+1}^-) = \Phi(t_{k+1}, t_k)\hat{\mathbf{x}}(t_k^+) + B_d\mathbf{u}(t_k) \tag{2.5}$$

$$\mathbf{P}(t_{k+1}^-) = \mathbf{\Phi}(t_{k+1}, t_k)\mathbf{P}(t_k^+)\mathbf{\Phi}^T(t_{k+1}, t_k) + \mathbf{Q_d}(t_k). \tag{2.6}$$

where $\hat{\mathbf{x}}(t_k^+)$ is the post-measurement update state estimate at time t_k, $\hat{\mathbf{x}}(t_{k+1}^-)$ is the propagated (pre-measurement) state estimate at time t_{k+1}, $\mathbf{P}(t_k^+)$ is the post measurement filter covariance, and $\mathbf{P}(t_{k+1}^-)$ is the propagated filter covariance.

With the state estimates propagated, the next step is to combine the measurement data, when it is available, with the propagated state estimate. This is done using

$$\mathbf{z}(t_k) = \mathbf{H}(t_k)\mathbf{x}(t_k) + \mathbf{v}(t_k) \tag{2.7}$$

$$\mathbf{K}(t_k) = \mathbf{P}(t_k^-)\mathbf{H}^T(t_k)[\mathbf{H}(t_k)\mathbf{P}(t_k^-)\mathbf{H}^T(t_k) + \mathbf{R}(t_k)]^{-1} \tag{2.8}$$

$$\hat{\mathbf{x}}(t_k^+) = \hat{\mathbf{x}}(t_k^-) + \mathbf{K}(t_k)[\mathbf{z}(t_k) - \mathbf{H}(t_k)\hat{\mathbf{x}}(t_k^-)] \tag{2.9}$$

$$\mathbf{P}(t_k^+) = \mathbf{P}(t_k^-) - \mathbf{K}(t_k)\mathbf{H}(t_k)\mathbf{P}(t_k^-) \tag{2.10}$$

where $\mathbf{z}(t_k)$ is the measurement equation, $\mathbf{H}(t_k)$ is the output matrix, and $\mathbf{v}(t_k)$ is the measurement corruption noise, which is white and Gaussian [8]. The matrix $\mathbf{K}(t_k)$ is the Kalman Gain. This is a ratio that tells the filter how much weight should be applied to the filter estimate and to the measurement. For instance, if the system estimate has a large uncertainty in relation to the measured state values, then $\mathbf{K}(t_k)$ would drive the filter's post-measurement estimate, $\hat{\mathbf{x}}(t_k^+)$, towards a value closer to the filter's estimate prior to measurement incorporation, $\hat{\mathbf{x}}(t_k^-)$.

2.3.1.2 Kalman Filter Implementation For Nonlinear Systems. As mentioned earlier, the above KF equations are based on the assumption that the system dynamics are linear. However, systems operating in the real-world are seldom linear over all operating conditions. In order to meet this assumption, the system dynamics must be linearized. There are two different KF types that use linearization, the linearized KF (LKF) and the Extended KF (EKF) [7]. Each type uses the same procedure to linearize the dynamics equations, but differ in the operating point used to linearize about. The linearization procedure begins with a nonlinear system, described by Maybeck as

$$\dot{\mathbf{x}} = \mathbf{f}[\mathbf{x}(t), \mathbf{u}(t), t]. \tag{2.11}$$

The linearized KF is developed by calculating the Taylor series that describes this differential equation about some nominal condition and then ignoring the higher-

order terms [8]. For the general case presented here, the Taylor series expansion is found to be

$$\dot{\delta\mathbf{x}}(t) = \mathbf{F}(t)\delta\mathbf{x}(t) + \mathbf{B}(t)\delta\mathbf{u}(t) \tag{2.12}$$

where

$$\begin{aligned}
\mathbf{F}(t) &= \left.\frac{\partial \mathbf{f}}{\partial \mathbf{x}}\right|_{\mathbf{x}_o(t),\ \mathbf{u}_o(t),t} = \left.\begin{bmatrix} \frac{\partial f_1}{\partial x_1} & \cdots & \frac{\partial f_1}{\partial x_n} \\ \vdots & \ddots & \vdots \\ \frac{\partial f_n}{\partial x_1} & \cdots & \frac{\partial f_n}{\partial x_n} \end{bmatrix}\right|_{\mathbf{x}_o(t),\ \mathbf{u}_o(t),t} \\
\mathbf{B}(t) &= \left.\frac{\partial \mathbf{f}}{\partial \mathbf{u}}\right|_{\mathbf{x}_o(t),\ \mathbf{u}_o(t),t} = \left.\begin{bmatrix} \frac{\partial f_1}{\partial u_1} & \cdots & \frac{\partial f_1}{\partial u_n} \\ \vdots & \ddots & \vdots \\ \frac{\partial f_n}{\partial u_1} & \cdots & \frac{\partial f_n}{\partial u_n} \end{bmatrix}\right|_{\mathbf{x}_o(t),\ \mathbf{u}_o(t),t}
\end{aligned} \tag{2.13}$$

and $\mathbf{x}_o(t),\ \mathbf{u}_o(t), t$ are the nominal conditions. The complete derivation of these equations can be viewed in [8].

Using this method, there are two options for choosing the nominal conditions. The first method is to design the KF to use a dynamics matrix that does not change after the initial linearization, meaning $\mathbf{f}(t)$ is linearized about a known nominal trajectory or about a set of conditions known to be marginally nonlinear [7]. This is the LKF. The second method relinearizes the dynamics matrix about each filter estimate. This method, used in the EKF, takes into account the fact that the filter is providing the optimal estimate at any given time, which makes this method more accurate in cases where a nominal trajectory is not known in advance or when the system varies in a highly nonlinear fashion [7]. An example of the differences in performance between these two methods can be viewed in [7].

2.3.2 Magnetic Field Based Navigation. Magnetic fields have been observed by humans for centuries. Plato wrote of rocks that were magnetically attracted to other rocks in 400 BC [1]. The Chinese developed a magnetic compass between 300 and 200 BC that was used to align construction with the Earth's magnetic fields; this

compass was made to look like the big dipper, so that the end of the bowl would point in the horizontal northward direction, also like the big dipper [1]. From these early observations and uses, merchants began using compasses to navigate to their various trading locations. This was the start of the compass navigation used to today. Compasses use the magnetic properties of repulsion and attraction to determine which direction is north relative to the users current position. As demonstrated by Columbus and many other early explorers, not understanding the nature of the Earth's magnetic field can cause confusion when trying to use the Earth's magnetic field to navigate on the Earth [1].

2.3.2.1 Brief Description of the Earth's Magnetic Field. Magnetic north, or the point that compasses point to, is currently offset from the geographic north pole, or the Earth's spin access, by about 12° in latitude [1, 14]. However, the pole location is not stationary, which causes the location of magnetic north to rotate around the geographic pole every 2,000 to 3,000 years [1]. This offset is caused by the nature of the Earth's magnetic field.

The Earth's magnetic field is often viewed as a large dipole magnet, that is a magnet that has two opposing poles (generally termed north and south poles) at each end [1]. Campbell points out that the Earth's magnetic field acts like a dipole, but is not actually a dipole magnet. The magnetic field that surrounds the Earth comes from currents that are induced by "the outer-core region of the Earth", which is composed of "a hot and dense liquid of highly conducting nickel-iron", and "the Earth's spin and shape" [1]. Together these characteristics form a current-loop that generates a magnetic field that acts similar to a dipole magnet. Figure 2.2 shows the different layers of the Earth, as well as the magnetic field surrounding it [1]. From this illustration, it can be seen that the Earth's magnetic field can be observed from any position on the Earth. While the main field of the Earth's magnetic field is fairly constant, there are a number of factors that can cause variation in the intensity of the magnetic field at any given time and place.

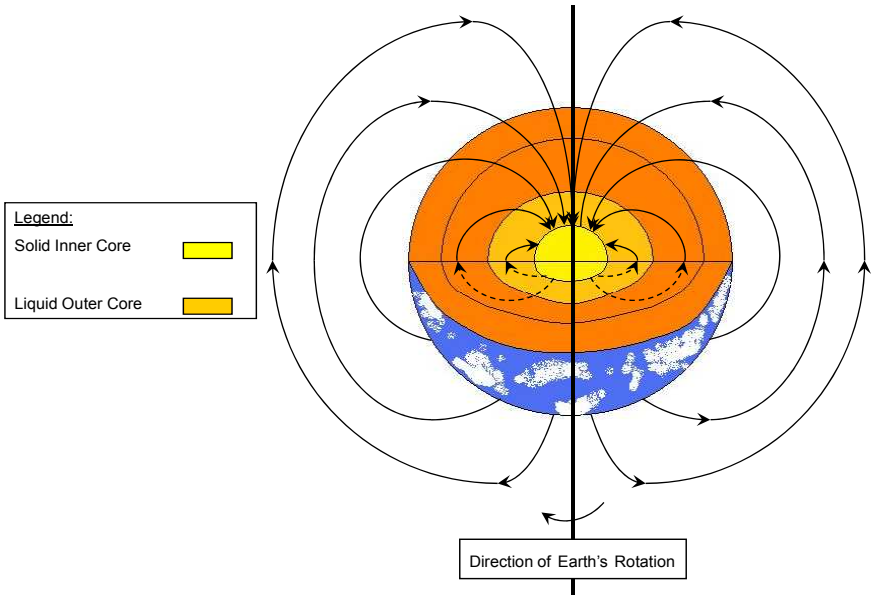

Figure 2.2: Illustration of the Earth's main dipole magnetic field. The liquid outer core, along with the Earth's rotation is believed to be the source of the Earth's dipole like magnetic field [1].

Campbell highlights two of the naturally occurring variations. The first is caused by an alteration in the Earth's electrical conductivity, which can be caused by "a major change in the groundwater content at a deep subsurface fracture...or when a highly conductive active magma chamber at a volcanic site moves before an eruption" [1]. The second cause is a result of a change in the magnetic domain boundaries of rocks due to increased external stress [1]. Campbell describes this by stating this change is brought about "as a result of the loading of rock surfaces as a major dam is filled or at a volcano as a result of a change in the magma chamber pressure on the surrounding rock material" [1].

In addition to variations of this nature, deposits in the Earth's crust also contribute to local variations in the observed magnetic field [10,19]. These local variations have more of an effect closer to the Earth's surface. As altitude is increased, the intensity of the magnetic field has less variation due to these deposits in the crust [10, 19].

Some other factors that can add to these variations are the effects on the Earth's magnetic field due to magnetic storms, the moon, the sun, and the ionosphere [10].

There are also artificial disturbances that perturb the Earth's magnetic field [10]. These artificial disturbances are caused by electrical currents running through any type of metal or conducting structure. In buildings, walls are often reinforced with steel rebar, newer construction projects use steel studs in interior walls. Steel beams used to support the floors of buildings add to the problem, as well as pipes, wires, and electric motors or equipment [10, 13].

2.3.2.2 Biological Examples of Magnetic Field-Aided Navigation. The Earth's magnetic field, as described in Section 2.3.2.1 is used by a number of animals to help them find their way to mating areas, migration locations, and moving around their habitats [6]. Two animals that are known to use the Earth's magnetic field to gain positional information during their long-distance migrations are the loggerhead sea turtle and the pied flycatcher [6].

The loggerhead sea turtles migrate from their hatching location along the east coast of Florida to an area called the North Atlantic gyre and then back to the south-eastern United States [6]. Experiments conducted by Lohmann and Lohmann showed that loggerhead turtles can measure the magnetic inclination angle of the Earth's magnetic field and the magnetic field intensity [6], and that they use this to help them navigate. The central European pied flycatcher's begin their migration in central Europe and then fly a course that prevents them from having to cross areas that are not conducive to survival (i.e. the Alps, the Mediterranean Sea, and the central Sahara) [6]. The path taken by these birds has them fly in a southeasterly direction and then, at a specific point, turn and continue their migration. The experiment used to investigate this phenomenon used the magnetic fields associated with the various locations along the path of their migration [6]. The result was the pied flycatchers turned to the same direction, and the direction of their normal migration route, when

the magnetic field was artificially changed to match that of the true magnetic field at the location where a heading change would normally occur [6].

These are just two examples of animals naturally using the characteristics of the Earth's magnetic field to navigate their way around the Earth. Several other animals have undergone the same sort of experiments and the use of magnetic fields has been shown [6]. These studies have helped humans to better understand how animals navigate around the globe and given researchers ideas for new methods of navigation using the Earth's magnetic field as a source for position and attitude information.

2.3.2.3 Navigation Techniques Using the Earth's Magnetic Fields. Early on in global explorations, explorers believed that their compasses pointed to a "magnetic mountain" [1], as opposed to a magnetic field generated by the composition of the Earth. As Spanish merchants began to move outside of "a narrow longitudinal sector along the west coast of Africa", it became obvious that this "magnetic mountain" was not a true stationary mountain aligned with true north as previously thought [1]. This observation led scientists to begin examining the true nature of the observed magnetic field. Based on their studies, new methods of navigation were developed. One of these breakthroughs was the use of declination angles to account for the observed difference between magnetic north and true north. These are angles that can be added (or subtracted) to the magnetic north heading to find the heading for true north. For maritime applications, as the ship experiences changes in longitude, the declination angle will also change [1]. To keep track of this, the declination angles must be known for all locations along the path of travel. This advance allowed for explorers, merchants, and anyone else wanting to navigate using a compass and map to accurately find their destination. This type of navigation is still taught today and is effective when GPS is not available and in environments where a compass will provide accurate readings.

Magnetic fields are also used to determine which direction a vehicle is facing, also known as its heading. This is an important tool as vehicles become smaller because

heading measurements generally come from gyroscopes, and accurate gyroscopes are generally bulky [16]. For outdoor applications, this type of aiding is very effective, assuming the declination angle is known. For indoor applications, the use of electronic compasses is not as straight forward. As mentioned in Section 2.3.2.1, there are many disturbances present in the indoor environment. While there are a number of different ways to reduce the impacts of these disturbances, the heading provided in indoor applications still does not meet the accuracy needs of many indoor applications [13].

It is apparent that there are many different ways to use the Earth's magnetic field in navigation. However, each of the above methods are impacted by variations in the Earth's magnetic field. Titterton and Weston suggest using a map of magnetic anomalies to estimate the vehicle's position [16]. This method relies on magnetic anomaly maps and the stability of such anomalies. However, since the anomalies are the measurement, the anomalies will not interfere with the measurements like when using an electronic compass indoors for heading reference [13]. Instead, assuming they are stable, or vary in a quantifiable way, the more variations in a given location, the more unique the magnetic "fingerprint" [3]. Figure 2.3 shows an example of this "fingerprint" for an indoor environment.

This technique has been demonstrated in the outdoor environment on an aircraft [19]. Wilson, Kline-Schoder, Kenton, Sorenson, and Clavier use maps of "aeromagnetic anomalies", which are found by taking the difference of the expected magnetic magnitude and the actual measured local field [19]. The approach outlined in [19] uses only the magnitudes of the magnetic field anomaly vectors. By doing this, Wilson et al. do not take advantage of all the information available from the magnetic field. The experiment is conducted using a three-axis magnetometer, but the three measured values are then combined to find the total magnitude of the magnetic field. The terrain navigation approach outlined in the next section will show a way to use these three different values together, in order to come up with a position solution.

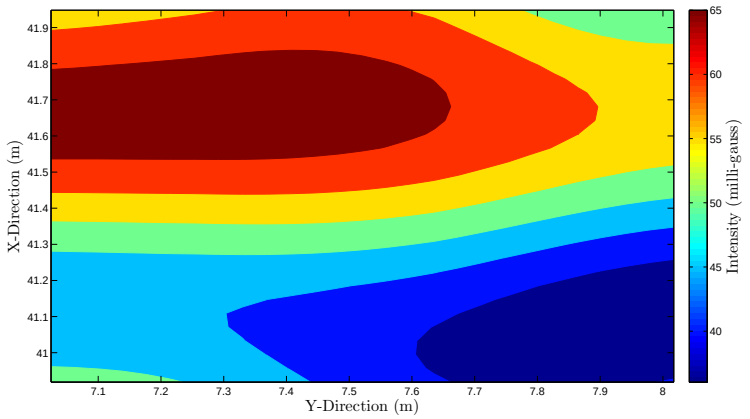

Figure 2.3: Map of a one square meter magnetic fingerprint generated from magnetic field data collected in a hallway at the Air Force Institute of Technology.

2.3.2.4 Magnetic Field Navigation Using a Terrain Navigation Approach.

Terrain navigation, in general, is based on measuring the terrain topography and then correlating this measurement with a position on a map [11]. The depth or height measurements often used in these methods are similar to the magnitudes of the magnetic field. Early methods of terrain navigation used single beam measurements to determine the location; this method was not very accurate in flat-bottomed areas, which do not have enough variation to determine the location of the measured position [11]. Modern terrain navigation methods use many more beams to measure a broader area, which provides more information; hence making it easier to pinpoint the vehicle's position [11]. The terrain navigation approach described by Nygren in [11] describes a method for combining multiple depth measurements with some sort of navigation system (i.e. INS, Doppler velocity log (DVL), or a system that measures how far the submarine has traveled by counting propeller turns) to determine a submarine's position.

Nygren's method begins by defining the system model as

$$\mathbf{x}_{t+1} = \mathbf{x}_t + \mathbf{u}_t + \mathbf{v}_t; \qquad t = 0, 1, 2, \cdots \tag{2.14}$$

$$\mathbf{y}_t = \mathbf{h}(\mathbf{x}_t) + \mathbf{e}_t \tag{2.15}$$

where $\mathbf{u}_t$ is defined as the displacement from the previous position, $\mathbf{x}_t$, at time t, $\mathbf{v}_t$ is the random error associated with the navigation system that provided $\mathbf{x}_t$, $\mathbf{h}(\mathbf{x}_t)$ is the function that maps a specific value of $\mathbf{x}_t$ to the measurement domain, and $\mathbf{y}_t$ is the actual measurement collected by the sensor, which has a measurement error, $\mathbf{e}_t$ [11]. Equation 2.14 is defined as the propagation equation and Equation 2.15 is the measurement equation [11]. These equations can be combined using methods similar to those discussed in Section 2.3.1.

If $\mathbf{e}_t$ is Gaussian, the likelihood function is

$$L(\mathbf{x}_t; \mathbf{y}_t) = \frac{1}{\sqrt{\left((2\pi)^N \sigma_e^2\right)}} exp\left(-\frac{1}{2\sigma_e^2}\sum_{k=1}^{N}\left(y_{t,k} - h_k(\mathbf{x}_t)\right)^2\right) \tag{2.16}$$

where σ_e^2 is the measurement error variance and N is the number of measurements to be incorporated [11]. Equation 2.16 is a mathematical way to determine how well a measurement correlates to the information contained in the map [11]. Therefore, the maximum value of $L(\mathbf{x}_t; \mathbf{y}_t)$ is located at the point most likely to be the position of the vehicle. Nygren points out that if this information is used by itself, then the position estimate is considered a maximum likelihood estimate (MLE). For the case of the submarine, or any vehicle with an additional navigation system, the MLE can be combined with the position estimate from the propagation equation using Bayes' rule [11]. As defined in [5], Bayes' rule is

$$P\left[B|A\right] = \frac{P\left[A \cap B\right]}{P\left[A\right]} \tag{2.17}$$

which can be written equivalently as

$$P\left[B|A\right] = \frac{P\left[A|B\right]P\left[B\right]}{P\left[A\right]}. \tag{2.18}$$

where $P[A|B]$ is the probability of A given all values of B.

For the application in [11], $P[B|A] = p(\mathbf{x}_{t+1}|\mathbf{Y}_{t+1})$, $P[A|B] = L(\mathbf{y}_{t+1}|\mathbf{x}_{t+1})$, $P[B] = p(\mathbf{x}_{t+1}|\mathbf{Y}_t)$, and $P[A]$ becomes a normalizing constant, C, to ensure the result integrates to one. The result of this is that the posterior probability density function (pdf), meaning the pdf associated with the position estimate after the position measurement is incorporated, is found by combining the propagated position pdf with the result of Equation 2.16. Mathematically, this can be written as

$$p(\mathbf{x}_{t+1}|\mathbf{Y}_{t+1}) \sim \frac{L(\mathbf{y}_{t+1}|\mathbf{x}_{t+1})\, p(\mathbf{x}_{t+1}|\mathbf{Y}_t)}{C}. \tag{2.19}$$

Once the posterior pdf is found, the position measurement can be calculated using the point of maximum likelihood, found using Equation 2.16, as the position measurement and the uncertainty associated with this position measurement, R, is the radius of curvature of the posterior pdf at the point of maximum likelihood [11]. Then, as outlined by Nygren and using the KF techniques discussed in Section 2.3.1, the position estimate is updated using this measurement data.

2.4 Summary

This chapter has shown why position aiding of inertial systems is necessary for navigation. It has also described the nature of the magnetic fields that are present outdoors and indoors, as well as the nature of the disturbances that create variations in these fields. Numerous applications of using magnetic fields for navigation were presented, followed by an introduction to the approach used in this research. Chapter III will describe the methodology used to develop the magnetic aided position algorithm used in this research.

III. Methodology

This chapter will step through the design process that was used for creating a magnetic field aided navigation system. The design process begins with having the necessary hardware and software to complete the data collection and the navigation algorithm because the first piece of required data for the design process is the magnetic field intensity map. Without this initial data collection, feasibility of the approach could not be verified. Therefore, this chapter will describe how the area to be mapped was setup, as well as how the magnetic field intensity map was constructed from the magnetic field intensity information. Once the map description is complete, the system model is defined and used to generate the propagation equations that are required for implementation of the KF. Following the development of the propagation equations, the algorithm for generating the position measurement is detailed. The KF update equations are then outlined.

With the basic aiding algorithm described, the next portion of this chapter covers the implementation of a leader-follower algorithm. This algorithm uses a lead vehicle to measure the magnetic field as it passes through an area. The lead vehicle then passes the magnetic field data, its estimated trajectory, and any turn commands to the follower vehicle. The follower vehicle then traverses the same area using only the provided data and a motion measurement device. The designed magnetic field aiding algorithm is used in conjunction with the data from the lead vehicle.

3.1 Required Equipment

One of the first steps in collecting and processing data is to be certain that equipment is available and that it will meet the requirements of the design. For this research, the only required equipment is three three-axis magnetometers and a laptop that can collect and process all data pertaining to the magnetic field intensity map and the magnetic aided position algorithm.

3.1.1 Three-Axis Magnetometers. Initially, the three-axis magnetometers present in the MIDG II® were analyzed for their use as the magnetometers in this research. However, the specifications for the MIDG II® magnetometer were not available from the manufacturer. While the magnetometer data is easily accessible through the device interface, it is only intended to aid the heading information in the INS by providing the direction of the magnetic field intensity vector, but not the magnitude [15]. Therefore, it is not meant to be a stand-alone magnetometer and very susceptible to temperature fluctuations and the readings might not be stable over long periods of operation. Due to the design requirements of the device, the magnetic readings produced by the MIDG II® cannot be converted to a standard unit of measure. In addition to not accurately measuring the magnitude of the magnetic field vector, the readings from each MIDG II® magnetometer were corrupted by scale factor errors and biases. These errors could be accounted for using the least-squares approach, but when the sensors were rotated 90°, the readings on the sensor did not reflect such a rotation (i.e., if the x-axis reading was 900 counts, when rotated 90° the y-axis should read 900 counts (using a standard right-handed Cartesian coordinate frame)). Without being able to accurately account for this error a different sensor was required.

The three-axis magnetometer used for this research was the Honeywell HMR2300®. The HMR2300® is a stand-alone three-axis magnetometer designed to provide magnetic field intensity information for a number of applications. Figure 3.1 shows the HMR2300® as used in this research. The HMR2300® has a measurement range of ± 2 gauss with a resolution of < 70 μgauss [4]. For reference purposes, the Earth's magnetic field ranges from approximately .3 gauss at the equator to .6 gauss at the poles [14]. Based on the magnitude of the Earth's magnetic field intensity, the selected magnetometers should be able to measure all variations about the Earth's main field.

3.1.2 Laptop. The laptop used in this research was a Dell® Latitude D630 with an Intel® Centrino® 2.0 GHz processor. Overall, it is a standard notebook

Figure 3.1: Photo of the Honeywell HMR 2300 as packaged for research

personal computer. `LabVIEW`® was used to collect the magnetic field intensity data and `Matlab`® was used to complete all data processing in a post-processing mode.

3.2 Magnetic Field Intensity Map

As mentioned in Section 2.3.2.4, a map of the magnetic field intensities must exist in order to use the terrain navigation approach. The map must contain location specific magnetic field intensity data. This section will describe the two main steps taken to generate these maps of magnetic field data. The first step covers the data collection methods, while the second outlines the process used to transform the measured data into a useable format.

3.2.1 Magnetic Map Data Collection. Following the approach used in [11], the map data is actually a grid of measurements at specific locations. The environment chosen to demonstrate this technique was two connected hallways near the Advanced Navigation and Technology Center at the United States Air Force Institute of Technology (AFIT). Figure 3.2 is a blueprint of the area used for this experiment, with the actual hallways used outlined in red.

A right-handed, Cartesian reference frame is used in the development of the algorithm, with the Z-axis being positive in the downward direction. Figure 3.2 shows the navigation reference frame in relation to the hallway and Figure 3.3 shows the navigation reference frame with respect to the body reference frame. The positive

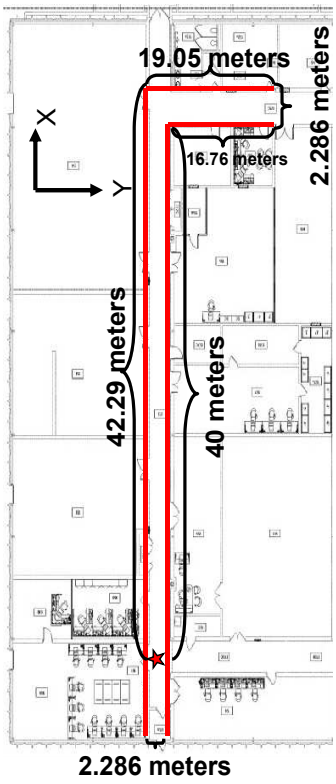

Figure 3.2: Layout of test environment used for testing magnetic-aided INS. The area is a hallway at the Air Force Institute of Technology.

X-axis is considered forward from the starting location (which is denoted by a star in Figure 3.2), while the Y-axis extends from left to right. Using this orientation, the grid spacing along the X-axis of the hallway needs to have the same spacing as the sensors to ensure the grid points line up with the grid points generated for the side hallway. To achieve the symmetric grid needed to build the map, the magnetometers are arranged in a row, with .381 meters (15 inches) of separation between each sensor. Therefore, the spacing between grid points, in both the X-direction and Y-direction, is .381 meters. To ensure position accuracy, a tape measure was used to place pieces of masking tape every .381 meters in the X-direction, and then every .381 meters in the Y-direction down the side hallway. The uppercase X, Y, Z denote the navigation frame, whereas, described in the following section, lowercase x, y, z denote the body's reference frame (the magnetometers are aligned with the body frame). As shown in Figure 3.3, when the angle ψ is 0°, the two reference frames are aligned.

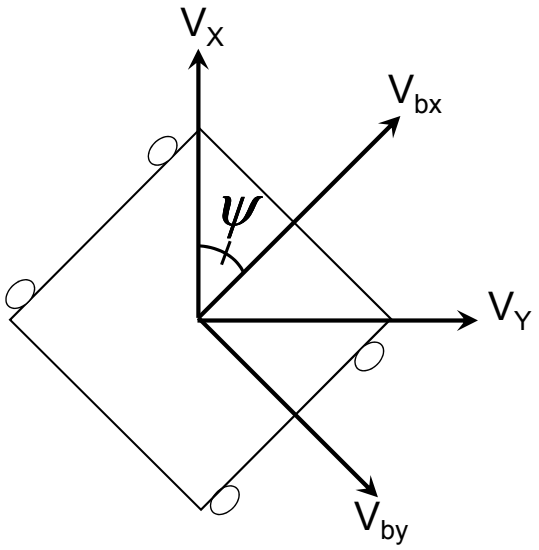

Figure 3.3: Relationship between the navigation reference frame and the body reference frame.

The actual grid data was collected using the cart and sensor array shown in Figure 3.4. A makeshift plumb-bob was used to ensure that the sensor array was aligned with the grid point. Once aligned, a reading was taken and stored in a text file. Due to the width of the hallway, the sensor array only covers half of the hallway. Hence, this procedure is completed twice for the main hallway and twice for the side hallway, resulting in a measurement being taken at 310 different locations, which amounts to 930 grid points of magnetic field intensity data. At each point, a full 3-axis magnetometer reading was taken. With the data collected in a data array, the next step is to turn this information into useful map data.

3.2.2 Magnetic Map Data Processing. Each three-axis magnetometer sends its magnetic field intensity data as a package. Table 3.1 shows a subset of the data collected using the magnetometers with labels to illustrate the data structure. By loading this information into `Matlab`® , the data can be reorganized to generate three different magnetic field intensity maps, one for each axis.

Figure 3.4: Photo of the data collection vehicle. Sensor array is located on board in front of the laptop.

As shown in Figure 3.2, the area to be mapped is L-shaped. In order to convert the magnetic data into a rectangular grid for `Matlab`® purposes, the measurements from the side hallway must be transposed and then aligned with the main hallway data. The area below the side hallway, but next to the main hallway, is unmapped and zeros are assigned to this region. Table 3.2 illustrates the resulting data structure.

When using grid points as a reference of position, the smaller the grid spacing the better. However, measuring a large number of grid points is time consuming and sometimes prohibited by measurement devices. In order to achieve a smaller space between measured grid points, the `Matlab`® *interp*() function is used to resample the collected data at a closer interval. By using the *interp*() function, the grid spacing is reduced from .381 m to .0381 m in all directions. Interpolating this data is valid because only a few points are needed between the existing points and, from Table 3.1, the variation between points appears to be fairly smooth.

3.3 System Model

As mentioned in Section 3.2.1, the reference frame used is not the body frame of the vehicle. Instead, the relationship between the navigation reference frame and

Table 3.1: Example of measured magnetic fields. This data is loaded into `Matlab`® and manipulated to form three magnetic field intensity maps, one for each axis. The units of the measured data is *counts* (1 *gauss*=15,000 *counts*). Each data point is separated by .381 meters (15 inches).

Left Sensor			Center Sensor			Right Sensor		
x-Axis	y-Axis	z-Axis	x-Axis	y-Axis	z-Axis	x-Axis	y-Axis	z-Axis
372	1442	3802	462	824	3067	1594	1671	4008
394	1447	3833	427	824	3081	1267	1744	3931
445	1514	3858	458	897	3103	1344	1968	3999
525	1587	3859	553	983	3123	1519	2017	4073
481	1020	2816	476	1045	3103	1423	2005	4069
394	1677	3844	451	1103	3062	1352	2233	3955
405	1667	3820	526	1111	2997	1638	2196	3920
383	1629	3804	530	1022	2955	1884	1520	3849
390	1595	3824	486	988	2958	1280	1847	3760
413	1595	3855	506	1042	3013	1494	2087	3891

Table 3.2: Data structure following reorganization to place data in positions that correlate to their true positions in the test environment.

	Side Hallway Data
Main	000000000000000000000000
	000000000000000000000000
Hallway	000000000000000000000000
	000000000000000000000000
Data	000000000000000000000000
	000000000000000000000000
	000000000000000000000000

the body frame is

$$\begin{bmatrix} V_Y \\ V_X \end{bmatrix} = \begin{bmatrix} cos(\psi) & sin(\psi) \\ -sin(\psi) & cos(\psi) \end{bmatrix} \begin{bmatrix} V_{bY} \\ V_{bX} \end{bmatrix} \tag{3.1}$$

where V_Y and V_X are the velocities in the direction of the Y and X axes in the navigation frame, V_b is the velocity of the vehicle in the body frame and ψ is the heading angle of the body with respect to the navigation frame. The relationship between the body frame and the navigation frame can be seen in Figure 3.3. For this research, the heading (ψ) is assumed known at all times.

Therefore, the system model of the experimental vehicle is defined, in the navigation reference frame, as

$$\underbrace{\begin{bmatrix} \dot{P}_Y \\ \dot{P}_X \\ \dot{V}_Y \\ \dot{V}_X \end{bmatrix}}_{\dot{\mathbf{x}}} = \underbrace{\begin{bmatrix} 0 & 0 & 1 & 0 \\ 0 & 0 & 0 & 1 \\ 0 & 0 & 0 & 0 \\ 0 & 0 & 0 & 0 \end{bmatrix}}_{\mathbf{F}} \underbrace{\begin{bmatrix} P_Y \\ P_X \\ V_Y \\ V_X \end{bmatrix}}_{\mathbf{x}} + \underbrace{\begin{bmatrix} 0 & 0 \\ 0 & 0 \\ 1 & 0 \\ 0 & 1 \end{bmatrix}}_{\mathbf{B}} \underbrace{\begin{bmatrix} u_{V_Y} \\ u_{V_X} \end{bmatrix}}_{\mathbf{u}} + \underbrace{\begin{bmatrix} 0 & 0 \\ 0 & 0 \\ 1 & 0 \\ 0 & 1 \end{bmatrix}}_{\mathbf{G}} \underbrace{\begin{bmatrix} w_{v_Y} \\ w_{v_X} \end{bmatrix}}_{\mathbf{w}} \tag{3.2}$$

where P_Y and P_X are the positions in the X and Y directions, u_{V_Y} and u_{V_X} are the control inputs used to control the velocity, and w_{v_Y} and w_{v_X} are the white, Gaussian noise driving the system, characterized by $E[\mathbf{w}(t)\mathbf{w}^T(t+\tau)] = \underbrace{\begin{bmatrix} \sigma_a^2 & 0 \\ 0 & \sigma_a^2 \end{bmatrix}}_{\mathbf{Q}} \delta(\tau)$.

3.4 Magnetic Aided Position Algorithm

The magnetic aided position algorithm is composed of three parts. The algorithm begins with the system propagation equations, followed by the position measurement generation algorithm, and then the measurement update equations. The propagation and update equations are the standard KF equations presented in Section 2.3.1, while the measurement generation algorithm uses the ideas presented in [11] and Section 2.3.2.4.

3.4.1 Propagation Equations. The propagation equations are found by applying the principles explained in Section 2.3.1, which begin with taking Equation 3.2 from the continuous-time domain to the discrete-time domain using a time step (Δt) of .1 *sec* and using $\sigma_a = .08\ m/s^2$. The resulting propagation equations are

$$\hat{\mathbf{x}}(t_{k+1}^-) = \underbrace{\begin{bmatrix} 1 & 0 & .1 & 0 \\ 0 & 1 & 0 & .1 \\ 0 & 0 & 1 & 0 \\ 0 & 0 & 0 & 1 \end{bmatrix}}_{\mathbf{\Phi}(t_{k+1},t_k)} \hat{\mathbf{x}}(t_k^+) + \underbrace{\begin{bmatrix} .005 & 0 \\ 0 & .005 \\ .1 & 0 \\ 0 & .1 \end{bmatrix}}_{\mathbf{B_d}(t_k)} \begin{bmatrix} u_{V_Y} \\ u_{V_X} \end{bmatrix} \tag{3.3}$$

$$\mathbf{P}(t_{k+1}^-) = \begin{bmatrix} 1 & 0 & .1 & 0 \\ 0 & 1 & 0 & .1 \\ 0 & 0 & 1 & 0 \\ 0 & 0 & 0 & 1 \end{bmatrix} \mathbf{P}(t_k^+) \underbrace{\begin{bmatrix} 1 & 0 & 0 & 0 \\ 0 & 1 & 0 & 0 \\ .1 & 0 & 1 & 0 \\ 0 & .1 & 0 & 1 \end{bmatrix}}_{\mathbf{\Phi^T}(t_{k+1},t_k)} + \underbrace{\begin{bmatrix} .0021 & 0 & .0320 & 0 \\ 0 & .0021 & 0 & .0320 \\ .0320 & 0 & .64 & 0 \\ 0 & .0320 & 0 & .64 \end{bmatrix} \times 10^{-3}}_{\mathbf{Q_d}(t_k)}. \tag{3.4}$$

Once the previous state estimate and covariance have been propagated forward in time, the next step is to use the propagated state estimate to generate a position measurement based on the magnetic field intensity measurement.

3.4.2 Measurement Generation. In terrain navigation, certain features or characteristics must be matched to determine the position and then that matched position is used as the position measurement for the KF. The same holds true when using magnetic field intensity data [3, 19]. The magnetometers measure the magnetic field intensity and then the measurement generation algorithm determines how this measurement relates to the vehicle's position via a mapping function [11].

Using the process outlined in Section 2.3.2.4, the first step in finding the position associated with a particular measurement is to combine the propagated pdf with the

result of the likelihood function to determine the location that best matches the magnetic reading. This is accomplished by:

1. Generating a discrete pdf that accurately describes the propagated position estimate.
2. Calculating the likelihood function for all possible locations.
3. Combining the results from steps 1 and 2 using Equation 2.19 to determine the position measurement, which is located at the maximum of the resulting pdf.
4. Calculating the measurement noise intensity, R.

3.4.2.1 Propagated PDF Generation. The propagated pdf contains all of the information about the propagated state estimate generated by the filter. For the two-dimensional Gaussian application, all necessary statistical information is contained in a bivariate Gaussian pdf, represented by its mean and standard deviation. These are computed as the propagated KF state estimate ($\mathbf{x}(t_k^-)$), and covariance $\mathbf{P}(t_k^-)$. Since the magentic field intensity data used in the likelihood function is discrete, the pdf must also be discrete to apply Bayes' rule. For a bivariate Gaussian pdf, the probability associated with a specific position on the pdf can be determined using this equation, modified from [8],

$$f_{\mathbf{x}}(\boldsymbol{\xi}) = \frac{1}{2\pi\sigma_Y\sigma_X\left(1-r_{YX}^2\right)^{1/2}} exp\left\{-\frac{1}{2\left(1-r_{YX}\right)^2}\left[\frac{\left(\xi_Y - x_Y^-\right)^2}{\sigma_Y^2} + \frac{\left(\xi_X - x_X^-\right)^2}{\sigma_X^2} - \frac{2r_{YX}\left(\xi_Y - x_Y^-\right)\left(\xi_X - x_X^-\right)}{\sigma_Y\sigma_X}\right]\right\} \tag{3.5}$$

where σ_Y and σ_X are the square roots of the associated terms from $\mathbf{P}(t_k^-)$, $x_Y(t_k^-)$ and $x_X(t_k^-)$ are the KF propagated filter estimates (mean values), r_{YX} is the correlation coefficient between the two random variables, and ξ_Y and ξ_X are the coordinates of the points where the probability is unknown. The discrete posterior pdf is then calculated by comparing all points (this is done by varying ξ_Y and ξ_X in Equation 3.5)

in a desired area to the filter estimate. In Matlab® , this can be done in a single step using an array of different ξ_Y and ξ_X.

3.4.2.2 Likelihood Function. In Equation 2.16, N is the number of different measurements to be used in determining the likelihood of a particular location. Since three-axis magnetometers provide three different magnetic field intensities, one along each axis, $N = 3$ for this application. Therefore, Equation 2.16 becomes

$$L(\mathbf{x}_t; \mathbf{y}_t) = \frac{1}{\sqrt{\left((2\pi)^3 \sigma_e^2\right)}} exp\left(-\frac{1}{2\sigma_e^2}\sum_{k=1}^{3}\left(y_{t,k} - h_k(\mathbf{x}_t)\right)^2\right). \tag{3.6}$$

By using the Matlab® capability to do math element-by-element in one command, the x-axis measurement, the y-axis measurement, and the z-axis measurement can be compared with their respective maps in one command. The result of this Matlab® command is an array of numbers that show how likely it is that a given location is the location of the vehicle, given the magnetic field intensity measurement. The next step in the process is to combine the propagated pdf with the result from the likelihood function.

3.4.2.3 Application of Bayes' Rule. As noted previously, the final step in determining the position measurement is completed by using Equation 2.19. The result from Section 3.4.2.1 and 3.4.2.2 make up the numerator of the right-hand side of Equation 2.19, repeated here for clarity. The maximum value of this data set, is the point that will be used as the position measurement, $\mathbf{z}(t_k)$, in the update equations.

3.4.2.4 Measurement Noise Intensity. From Section 2.3.1, it is known that the KF needs a value for the measurement noise intensity. For applications such as GPS, the measurement noise of the GPS measurement is the value assigned to R. In this case, that will not be sufficient because the measurements generated by the magnetometers are transformed into position measurements, but the errors are not directly transformed from gauss to a unit of length. In addition to the errors not being

in the proper units, any information that could be gained from the post-Bayes' rule pdf is dependant upon the filter's uncertainty and, for a KF, the process noise and the measurement noise (i.e., $\mathbf{Q}(t_k)$ and $\mathbf{R}(t_k)$, respectively) need to be uncorrelated or accounted for by an augmented state matrix. The method proposed by Nygren in [11] uses the radius of curvature of the posterior pdf to calculate R, but then augments the KF to account for this correlated noise. Instead of using the correlated noise method, a new method was developed to remove the correlation.

The new process begins with the point of maximum likelihood. Using this point as the center, an array of indices is created in the X-direction and in the Y-direction. The measured magnetic field intensity is then compared with the magnetic field intensities of the surrounding locations using Equation 3.6. The result of the likelihood function is then normalized to make the result a pdf. The standard deviations of the two resulting pdfs (one for the X-direction and one for the Y-direction) will be the square root of the measurement noise intensity, or the standard deviation of the dataset. For a Gaussian pdf, $\sim$68% of the data is included within a 1σ-band. To calculate the standard deviation of experimental pdfs, the point on the left side of the mean where $\sim$16% of the data is in the tail can be found and the same for the right tail. The distance that these two points are from the mean of the pdf are then averaged to calculate the standard deviation (σ_Y and σ_X) of the measurement noise intensity, resulting in $\mathbf{R} = \begin{bmatrix} \sigma_Y^2 & 0 \\ 0 & \sigma_X^2 \end{bmatrix}$.

3.4.3 Measurement Update Equations. Once the position measurement used for updating the KF estimate is calculated, the update portion of the KF remains the same as described in Section 2.3.1.1. The only difference is that Equation 2.7 is replaced by the position associated with the maximum value of the likelihood and propagated pdf combination. Essentially, the measurement generation algorithm described in Section 3.4.2 replaces the mapping function and measurement noise that are represented in Equation 2.7.

3.5 Leader-Follower Methodology

With the process for aiding a navigation system with magnetic field data developed, the next step is to investigate the feasibility of using the magnetic aided position algorithm in a leader-follower scenario. The leader-follower scenario is defined by having the first vehicle, the leader, move through an area while measuring the magnetic field intensity along its path. The second vehicle would come along some time later with the magnetic field intensity data from the leader, the trajectory estimate from the leader, and any turn commands that were executed by the leader. The leader is envisioned as being a vehicle that has several different sensors on-board to aid in its travel through the indoor environment, as well as three magnetometers. The second vehicle is envisioned as being a less equipped vehicle, with only one magnetometer and some sort of motion measuring device (e.g., INS, odometer, etc.). The method described in Section 3.4 is used as the basis of this leader-follower approach.

3.5.1 Map Generation. In Section 3.2, the map generated was composed of six different sensor measurements and covered a rectangular, equally spaced grid. For this application, the points of the map are generated according to where the leader estimates it has traveled (which is different from where it actually traveled). In order to accomplish this non-uniform grid, the `Matlab`® function *griddata*() can be used. The leader collects magnetic field intensity data at a regular interval. In this case, that interval is every .5 sec. Each magnetic field intensity measurement is recorded by the leader, along with the estimate of the leader's position at the time of measurement. The magnetic field intensity measurements and the leader's position estimate are sent to the follower vehicle. The follower vehicle compares its three-axis magnetometer measurements with those provided by the leader to determine where it is located in reference to the leader's estimated trajectory.

3.5.2 Follower Vehicle Control. The follower vehicle system model is similar to the system model presented in Section 3.3 except there is an additional control input, $\mathbf{u}_2(t)$. This control input is used to track the estimated trajectory of the lead

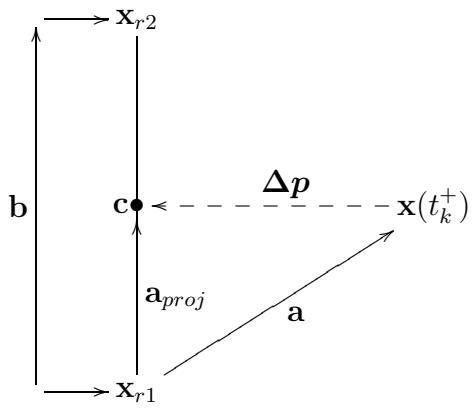

Diagram 3.1: Graphical example of the error ($\boldsymbol{\Delta p}$). The error $\boldsymbol{\Delta p}$ is used to determine the amount of control applied to the follower to track the reference trajectory $\mathbf{x}_r$

vehicle. Therefore, the stochastic differential equation used to describe the follower is

$$\dot{\mathbf{x}}(t) = \mathbf{F}(t)\mathbf{x}(t) + \mathbf{B}(t)\left(\mathbf{u_1}(t) + \mathbf{u_2}(t)\right) + \mathbf{G}(t)\mathbf{w}(t). \tag{3.7}$$

where the second controller, $\mathbf{u_2}(t)$, is a proportional integral derivative (PID) controller.

The PID controller was chosen because, as pointed out by Ogata in [12], PID controllers are applicable to most control systems and, after attempting a proportional controller, it became obvious that a different controller was needed. The PID controller combines a proportional controller with an integral controller and a derivative controller, which allows more flexibility in reaching various operating conditions. For a tracking controller, the setpoint error is found by calculating the error between the actual output of the plant and the reference trajectory. For this application, the goal is to ensure the follower navigates within the area mapped by the leader. Therefore, the cross-track error is the error that needs to be minimized. In order to calculate the cross-track error ($\boldsymbol{\Delta p}$), the distance between $\hat{\mathbf{x}}(t_k^+)$ and the leader's estimated trajectory must be found. The problem with calculating this error is that it cannot be directly calculated because the leader's trajectory is not defined for all points on the map. The geometry of the problem is shown in Diagram 3.1.

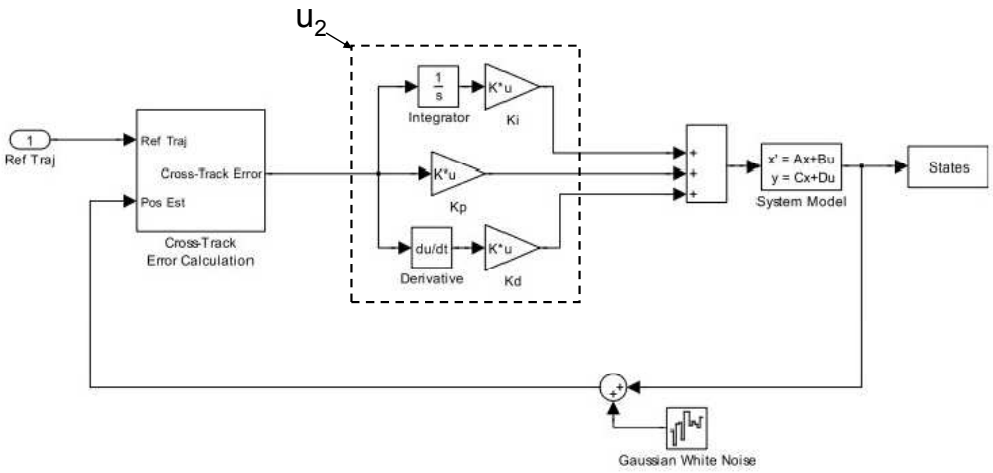

Figure 3.5: PID controller block diagram derived from [12] built in Simulink by `Matlab`®

Using Diagram 3.1 as a reference, the distance $\boldsymbol{\Delta p}$ is calculated by first finding the distance between $\hat{\mathbf{x}}(t_k^+)$ and $\mathbf{x}_{r1}$, which is the closest defined point on the reference trajectory located below $\hat{\mathbf{x}}(t_k^+)$. With the vector $\mathbf{a}$ calculated, the next step is to find the distance between $\mathbf{x}_{r1}$ and the point $\mathbf{c}$. This is completed by calculating $\mathbf{a}_{proj}$, which is the vector equivalent to $\mathbf{a}$ projected onto vector $\mathbf{b}$. By adding $\mathbf{a}_{proj}$ and $\mathbf{x}_{r1}$, the location of $\mathbf{c}$ is found. Once the value of $\mathbf{c}$ is found, $\boldsymbol{\Delta p}$ is found by subtracting $\mathbf{x}(t_k^+)$ from $\mathbf{c}$.

With the input to the controller defined, the final step in designing the PID controller is to determine the gain parameters that will ensure system stability and provide the desired performance. The PID controller uses three tunable gain parameters (K_p, K_i, and K_d) to achieve the desired system performance. By tuning these parameters, the response time of the system, the maximum overshoot, and the settling time can all be changed to meet system performance requirements.

Figure 3.5 is the block diagram of the total system used in the follower vehicle. The dashed box labeled u_2 is the PID controller. As mentioned previously, the input to the PID controller is the cross-track error.

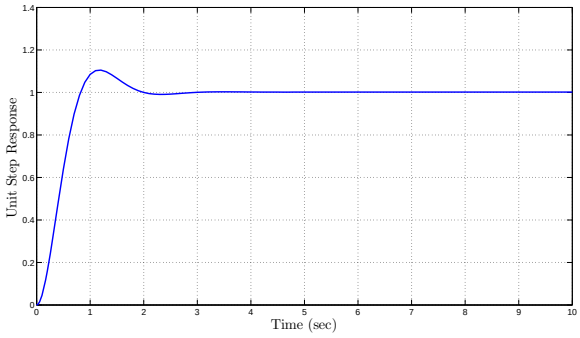

Figure 3.6: Step response of PID controller used to control the path of the follower, without process noise applied.

In this case, the controller gain values were found by using the `Matlab`® Simulink toolbox. The block diagram pictured in Figure 3.5 was executed in Simulink with varying values for the three gain parameters until the desired performance was achieved, which was a rise time less than 1 *sec*, with minimal overshoot (this was defined as less than .1 meters), and a settling time as close to 2 *sec* as possible. These values were achieved with $K_p = 10$, $K_i = .05$, and $K_d = 3.5$. The step response of this controller, with no process noise and $u_1 = \begin{bmatrix} 0 \\ 0 \end{bmatrix}$, is shown in Figure 3.6.

Figure 3.7 shows that the system will remain stable and track the desired trajectory when process noise is present. The noise that was added for this step response, was white, Gaussian noise with the same intensity, $\mathbf{Q}$, as that used in the system model introduced in Section 3.4.1. From these figures, it can be seen that the controller is stable and adequately meets the desired performance characteristics.

3.6 Summary

This chapter has described the procedures used to design the magnetic aided position algorithm. Chapter IV will show the results generated by implementing the processes and procedures explained in this chapter.

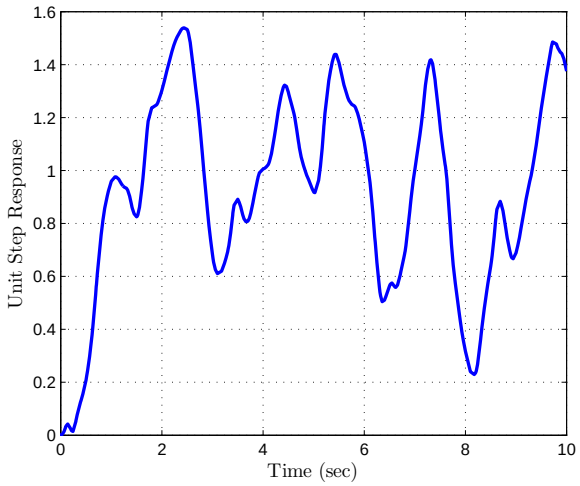

Figure 3.7: Step response of PID controller used to control the path of the follower, with process noise applied.

IV. Implementation

THIS chapter will show that the magnetic field variations are location specific, as well as discuss the performance of the magnetic aided position algorithm in environments that have small variations in the magnetic field. This was done using a simulation that uses both simulated measurements and real measurements. The simulated measurements were used to show the magnetic aided position algorithm's ability to track random trajectories, while the real measurements were used to demonstrate that magnetic variations are stable enough in time to be used in such an application. Following the analysis of the magnetic aided position algorithm, using the simulation, the results from the leader-follower implementation will be examined. It will be shown that the leader-follower implementation is more susceptible to areas of small variation, and some methods for minimizing these impacts are presented.

4.1 Magnetic Field Intensity Variations By Location

To verify that the magnetic field intensity is location-specific, three different datasets of magnetic field intensity were collected from different hallways around the AFIT campus. The readings from the magnetic sensors could be different based on actual magnetic field intensity in that area, as well as if the sensors were not moved through the test areas in the same orientation. An example of this (using a standard right-handed Cartesian coordinate system) would be a magnetometer's x-axis is aligned straight ahead and the reading along that axis is .6 milli-gauss, the reading along the y-axis is .45 milli-gauss. When the sensor is rotated 90 degrees to the right, the y-axis is now facing the direction the x-axis was facing initially. The reading along the y-axis would now read .6 milli-gauss, while the x-axis measurement would be -.45 milli-gauss. To show that the variations are due to the environment and not the orientation of the sensors, three different test environments were chosen. The first hallway chosen runs east to west and is on the second floor of an academic building. For this data collection effort, a single magnetometer was moved 15.24 meters (50 ft), from east to west, through the hallway. Figure 4.1 shows the relationship between the

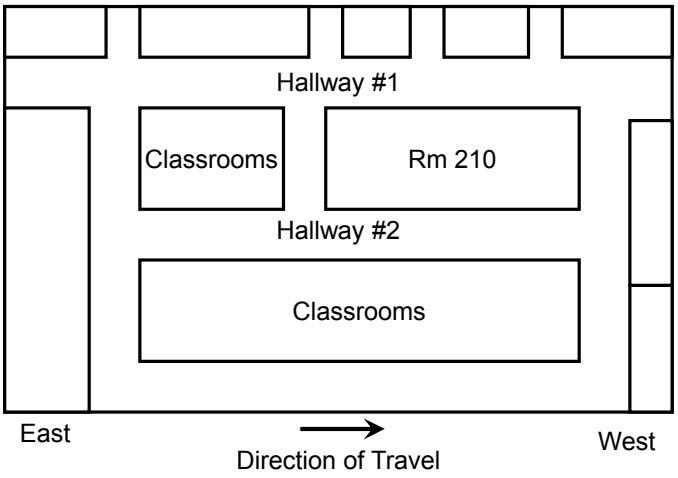

Figure 4.1: The orientations of the hallways used for demonstrating the uniqueness of magnetic field intensities in an indoor environment. Two are on the second floor and are parallel with each other, while the third is located on the third floor, directly above hallway number 1.

three hallways. The second hallway tested was chosen because it is located directly above the first hallway tested. Since the second hallway is oriented and in the same position as the first (except for the difference in height because one is on the second floor and the other is on the third), the data from these two hallways would be similar if the magnetic field intensities are not unique between locations. The third hallway was chosen to demonstrate the differences between two hallways that are on the same floor and aligned with each other. As can be seen in Figure 4.2, each of the hallways have their own unique magnetic fingerprints along each of the three magnetometer axes.

4.2 Magnetic Field Intensity Map

Based on the method described in Section 3.2, the magnetic field intensity maps have two main sections of data. The first is the magnetic field intensity data collected in the main section of the hallway, and the second data used is the magnetic field intensity data from the side hallway. The result of combining these two datasets can be viewed in Figure 4.3, which is a magnetic field intensity map generated from

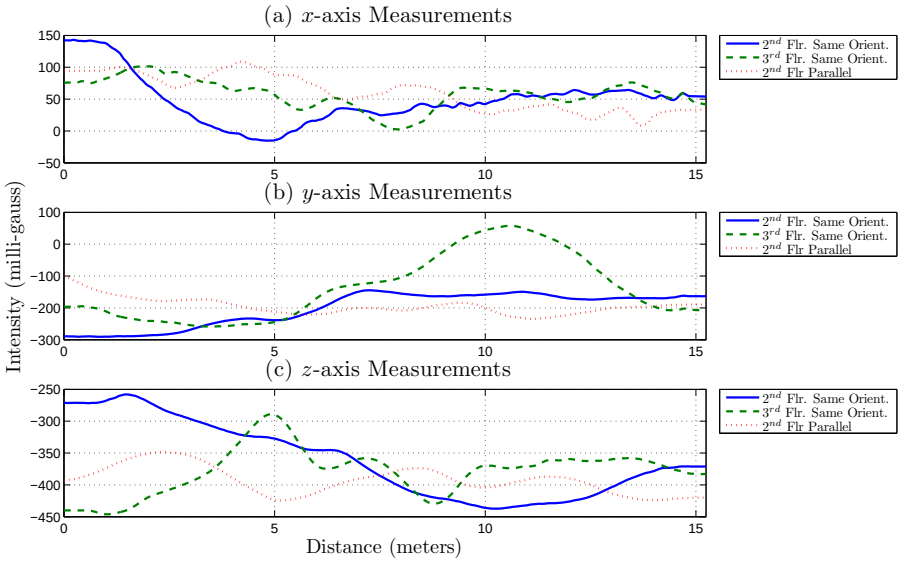

Figure 4.2: The magnetic field intensities in three different hallways, all oriented from north to south, were compared to show that each hallway has a unique magnetic field intensity fingerprint. The measurements were taken using one three-axis magnetometer.

the x-axis magnetometer measurements. The data extending along the X-axis is the data collected in the main hallway, while the data extending along the Y-axis is the side hallway data, with the exception of the zeros that are entered into the map as described in Section 3.2.2. While Figure 4.3 is a good illustration of how the data collected by the magnetometers is organized, it does not provide the required level of visual resolution to adequately analyze the information contained in the map. Therefore, the magnitude and variation of the data in the two hallways can be seen better when viewed separately.

4.2.1 Main Hallway Magnetic Field Intensity Map. Figure 4.4 shows the main hallway's magnetic field intensity map, using magnetic field intensity data collected on 20 November 2008. Since the magnetic aided positioning algorithm relies on differences in the magnetic field intensity to relate a magnetometer reading to a position, unique patterns and values of intensity are desired. For the HMR2300, the measurement noise has a standard deviation of approximately 25 counts, which equates to approximately 1.67 milli-gauss. Variations that are significantly larger than

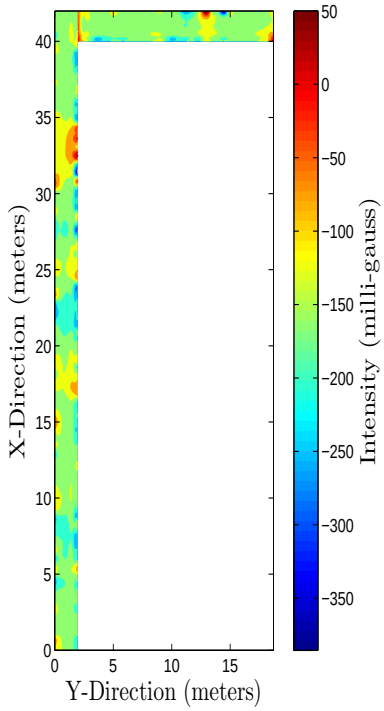

Figure 4.3: Example two-dimensional magnetic map using the x-axis magnetometer data.

1.67 milli-gauss will be largely unaffected by measurement noise. Due to the scale of Figure 4.4, it is difficult to ascertain how many variations are below this threshold. Figure 4.5 shows a smaller area of the hallway to increase the resolution. Based on Figure 4.5, the main hallway does have variations large enough to be seen over the magnetometer's noise.

4.2.2 Side Hallway Magnetic Field Intensity Map. Figure 4.6 was generated using the same procedures as the map for the main hallway. Overall, there are numerous variations present, but to see if the variations are sufficiently large, the same procedure applied to Figure 4.4 was applied to Figure 4.6. Figure 4.7 is the result of mapping a smaller section of the side hallway. The result is the same as that shown with the main hallway. There should be enough variation to determine distinct position information using the magnetic aided position algorithm. With the

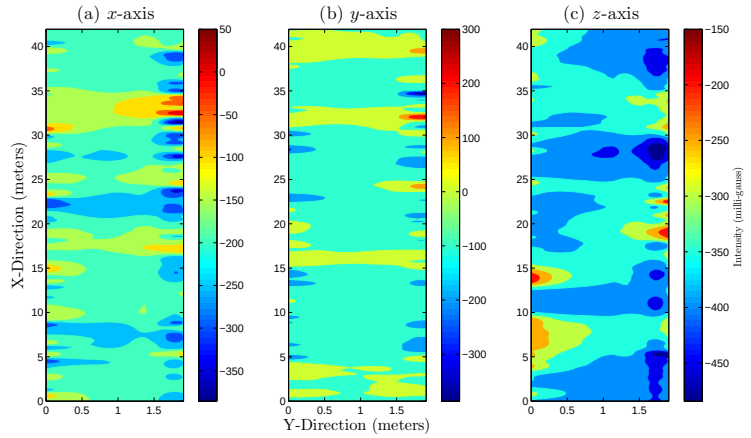

Figure 4.4: The main hallway magnetic intensity maps, generated per procedures outlined in Section 3.2. Each plot represents a different magnetometer axis.

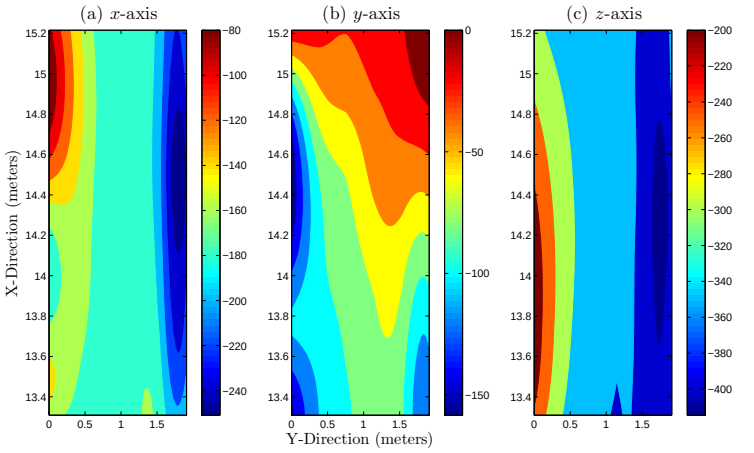

Figure 4.5: A closer look at the variations present in the main hallway. Variations smaller than 1.67 milli-gauss will not be visible above the noise of the magnetometer and could prevent the magnetic aided position algorithm from estimating an accurate position estimate.

map completed, the next step was to investigate the ability of the magnetic aided position algorithm defined in Chapter III to estimate a vehicle's trajectory.

4.3 Magnetic Aided Position Algorithm Results

This algorithm is implemented using two different approaches. The first approach uses a map of an entire area, which was measured ahead of time, to estimate the location of a vehicle within the mapped area. The second method uses magnetic field intensity data collected along a vehicle's path, as it moves through an area.

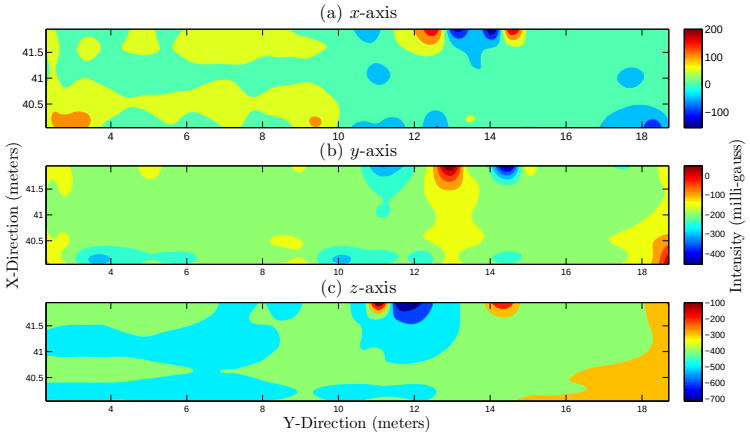

Figure 4.6: The side hallway magnetic intensity maps, generated per procedures outlined in Section 3.2. Each plot represents a different magnetometer axis.

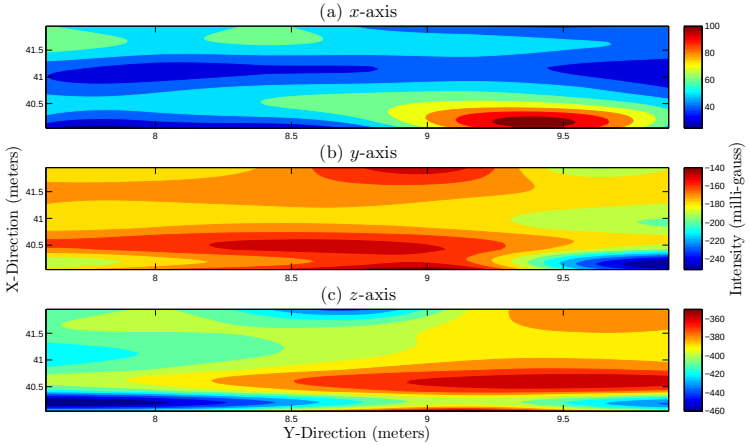

Figure 4.7: A closer look at the variations present in the side hallway. Variations smaller than 1.67 milli-gauss will not be visible above the noise of the magnetometer and could prevent the magnetic aided position algorithm from estimating an accurate position estimate.

The second method is used for a relative positioning solution (i.e., where is the second vehicle located with respect to the first), as opposed to an absolute positioning solution (where is the vehicle located in a defined area). The differences in these two methods only impact which method of map generation to use, as described in Section 3.2.2 and 3.5.1. Once the map is generated, the magnetic aided position algorithm uses the map in the same way to estimate a vehicle's position relative to the positioning system associated with the map.

4.3.1 Example Discrete Bivariate Gaussian PDF. As mentioned in Chapter III, the first step in the magnetic aided position algorithm is calculating the discrete bivariate Gaussian pdf. As mentioned previously, this pdf is centered around the propagated state estimate and uses the associated propagated filter uncertainties. For the example pictured in Figure 4.8, the position state estimate is $\hat{\mathbf{x}}(t_k^-) = \begin{bmatrix} 1.1565 \\ 2.2438 \end{bmatrix}$ and $\mathbf{P}(t_k^-) = \begin{bmatrix} 0.0513 & 0 \\ 0 & 0.4837 \end{bmatrix}$. The area in view was reduced to show more detail.

4.3.2 Example Likelihood Function Result. Using the same location as in the pdf case, Figure 4.9 shows the result of Equation 3.6. The measurements for this example were simulated based off of the truth data used in generating the map. For this example, it is clear that there are three peaks. Any one of these peaks could be the actual location of the vehicle. If the maximum value is chosen at this point this process becomes a maximum likelihood estimator [11]. However, this result is combined with the bivariate Gaussian pdf using Bayes' rule, as discussed in Section 3.4.2.3.

4.3.3 Example Bayes' Rule Implementation Example. The result of combining the likelihood function and the bivariate Gaussian pdf is shown in Figure 4.10. Since the two peaks of the likelihood function were so closely positioned, both are still present after combination with the pdf. However, the magnitudes of these peaks have been scaled according to their location from the filter's estimated position. The difference between the height of the peak located at approximately (1.75,1) and the one located at approximately (2.4,1) is now noticeably larger. Also notice that the peak located at approximately (1.5,3.2) is completely removed from the figure.

Choosing the point of maximum likelihood from the combination of the propagated pdf and the likelihood result could result in the wrong location being chosen. Choosing the wrong location could prevent the magnetic aided position algorithm from accurately estimating its position. For the basic trajectory estimation case to be presented, this phenomenon did not create a problem. However, in the leader-follower

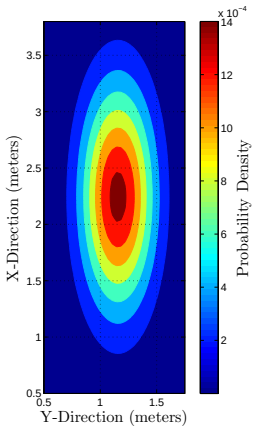

Figure 4.8: Example discrete propagated probability density function that will be combined with the result of the likelihood function using Bayes' rule.

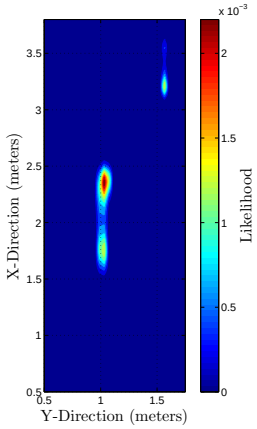

Figure 4.9: Example discrete likelihood function result that will be combined with the result of the discrete probability density function using Bayes' rule

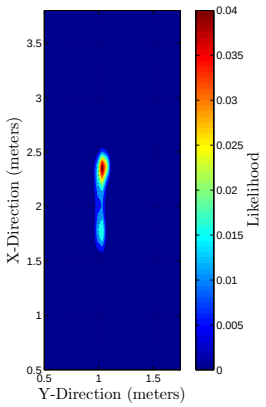

Figure 4.10: Example discrete post-measurement probability density function generated using Bayes' rule to combine Fig. 4.8 with Fig. 4.9.

implementation it did create a problem. In order to reduce the effects of bad measurements, several options could be implemented following the combination of the pdf and the likelihood function. One method would be residual monitoring. If a measurement was so many meters away from the estimate (this value would be determined based on your system model) that measurement would be ignored. Another method would be to ignore a measurement if there were multiple peaks within a pre-determined area, this area would be determined by the uncertainty of the system model.

4.4 Magnetic Field Aided Trajectory Estimation

Two tests were developed to demonstrate the concepts from Chapter III and the magnetic map information generated above. The first test consisted of two Monte Carlo simulations that used simulated measurements generated from the map data to estimate the trajectory of the vehicle. The second test used real magnetic field intensity measurements to estimate the trajectory of a vehicle. Both tests used the parameters shown in Table 4.1, with the exception of the vehicle starting position. The values shown in Table 4.1 for the vehicle starting location are the values used for the simulated measurements case. For the case with real measurements, there were two different starting points, (X_1,Y_1)=(0,1.524) and (X_2,Y_2)=(0,1.905), all in meters and with (0,0) being the bottom left corner of the hallway as oriented in Figure 3.2.

4.4.1 Generated Trajectory Simulation. There are three basic steps used in the Monte Carlo Simulations. The first step is the trajectory generation. Secondly, the magnetic field intensity measurements are calculated from the map data using the locations supplied by the generated trajectory (with an appropriate amount of measurement noise added). The final step in this simulation is implementing the KF with the system model and magnetic aided position algorithm developed in Sections 3.3 and 3.4. This simulated approach allows for large numbers of simulations to be executed, which aids in determining the filter's performance. If the simulation is representative of the actual system, Monte Carlo simulations show the expected performance of a system over a wide range of scenarios and conditions. For this implementation, taking measurements along 100 known trajectories is unrealistic with respect to time and instrumentation. The location of the magnetic measurement must be known when it is collected. Based on the measurement update interval of the filter, each trajectory requires 77 different measurements. This would amount to collecting 7700 different points of magnetic data. With the current test equipment, taking measurements for one trajectory (77 measurements) takes about 1 hour. A 100 run Monte Carlo simulation takes about 2 hours. At the very least, the Monte Carlo simulation will verify that the algorithm operates as intended, and it provides a baseline for comparison when real data is used. By understanding how the algorithm should perform under the best conditions, when the real data is used differences between the two can be used to determine areas of the simulation that do not accurately depict what is really happening or to help identify possible limitations of the algorithm. Once these limitations are understood, they can be investigated further to create a more representative simulation, which would provide a more accurate algorithm.

While a Monte Carlo simulation is a good tool for the reasons discussed, an understanding of its limitations is key to using this tool. The first key is to understand that there is never a true replacement for real data, but simulated data can work, in conjunction with real data, to aid in getting a more complete picture, without the time needed to collect large amounts of real data. If the simulation does not adequately

match the real system, the simulation results will be invalid and not provide useful information. In this case, if the measurement noise is not characterized correctly the simulation results would be inaccurate compared to the real data tests. Another area of the simulation that could be inaccurate comes from the fact that if the measurement data falls between grid points on the map, the magnetic measurement at that particular point is found by interpolating between two points that may have already been interpolated. While interpolation data is valid to some degree, as discussed in Section 3.2.2, interpolating interpolated data introduces another source of error into the system that is not modeled. With these differences understood, the next step is to describe the setup and show the results of implementing the Monte Carlo simulation.

4.4.1.1 Trajectory Generation. A nominal trajectory for this simulation was defined as down the center of the main hallway, then, following a 90° turn, down the center of the side hallway. The nominal trajectory is used to develop the dynamics model of the system, as described in Section 3.3. Using the process noise, as described in Section 3.3, the dynamics model is perturbed by white driving noise to create a random trajectory that is centered around the nominal trajectory. The initial attempt at generating this trajectory used $\sigma_a = .08\ m/s^2$. The initial attempt failed because the vehicle trajectory had no control to keep it within the confines of the hallway, which is physically impossible with a real vehicle. To overcome this physical reality, the trajectory was controlled to keep within the physical boundaries of the hallway. In addition to the control, if a trajectory was found to break the physical barrier of the hallway, it was rejected and the trajectory was regenerated. Figure 4.11 shows a trajectory generated using this method.

4.4.1.2 Simulated Magnetic Field Intensity Measurements. The magnetic aided position algorithm requires magnetic field intensity measurements. The measurements were generated from the magnetic field intensity data used to develop the magnetic field intensity maps mentioned previously. At each point along the generated trajectory, a magnetic field intensity was found by matching the trajectory

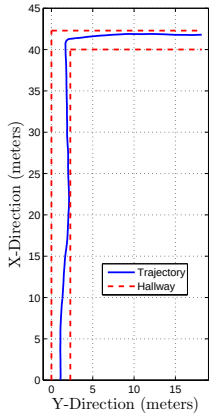

Figure 4.11: Example simulated trajectory used to test the filter's ability to track a random trajectory.

location with a location on the map of the hallway. If the data fell in between grid points, the magnetic field intensity was interpolated at that particular point. Once the true magnetic field intensity (the true magnetic field for this simulation was assumed to be the magnetic field intensity data collected for the construction of the magnetic field intensity map) was calculated for a given location, the white, Gaussian measurement noise was added to each measurement to simulate the measurement coming from a magnetometer.

4.4.1.3 Monte Carlo Results of Simulated Trajectories and Measurements.

Monte Carlo (MC) simulations are used to determine if a system or algorithm will operate as desired. For this research, 100 MC runs were completed using two different scenarios. Both scenarios used the magnetic aided position algorithm as described throughout this research. However, the first was executed without knowledge of the trajectory making the turn onto the side hallway, while the second used a control input to make the turn.

As seen in Figure 4.12, the positioning solution generated by the magnetic aided positioning algorithm achieves a root-mean-square (RMS) position error of less than .4 meters, when the filter is not supplied with turn information. When the turn command is provided to the filter, the RMS values (shown in Figure 4.13) drop below .2 meters once the initial positioning error is resolved. These two figures show that the

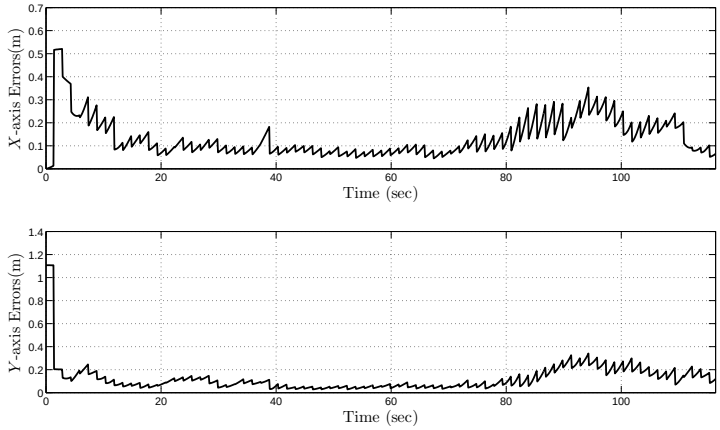

Figure 4.12: The RMS values for the magnetic aided position algorithm without a turn command provided to the filter. Notice the decrease in performance following the turn at approx. 80 seconds.

magnetic aided positioning algorithm is able to generate sub-meter level positioning solutions.

Figure 4.14 shows the ensemble mean position error, the ensemble standard deviation, and the RMS value of the filter uncertainties for all 100 MC runs, when no turn information was provided to the filter. Figure 4.15 shows the ensemble mean position error, the ensemble standard deviation, and the RMS value of the filter uncertainties. For reference, the turn takes place around 80 seconds, depending on the randomly generated trajectory. The mean error associated with this filter was calculated by subtracting the true trajectory from the estimated trajectory. Figure 4.14 shows that the magnetic aided position algorithm accurately estimates the vehicle's position uncertainty for the entire test environment. As mentioned in the beginning of Section 4.4.1, the goal of the MC simulation is to show that the magnetic aided position algorithm does operate properly. Generally, a KF is said to operate properly if the filter uncertainty accurately models the ensemble standard deviation of the results. The filter's estimate of the uncertainty tracks the ensemble standard deviation very well along the X-direction for both the filter that receives the turn command and the filter that does not, Figures 4.14 and 4.15 respectively. However, in both cases the Y-axis filter estimate is less optimistic in its estimate than the actual ensemble

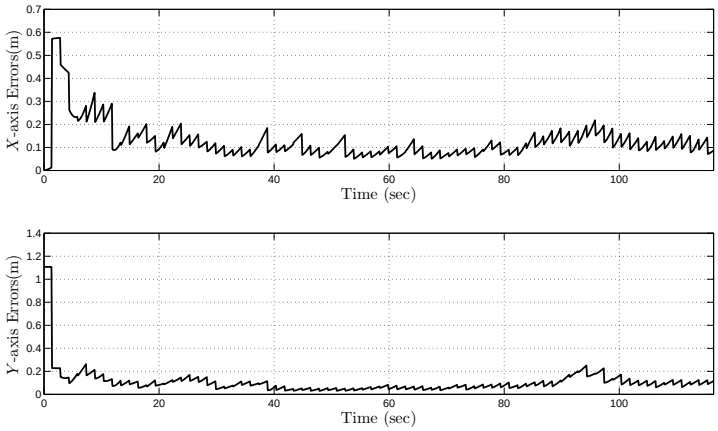

Figure 4.13: The RMS values for the magnetic aided position algorithm with a turn command provided to the filter. Notice the smaller decrease in accuracy following the turn.

statistics. While the estimation by both filters seems to not be impacted by this, both achieve sub-meter RMS errors, understanding this minor discrepancy is necessary to understanding how well the MC results relate to the real system.

The main source of the discrepancy between the ensemble standard deviation and the filter's uncertainty estimate was found to be due to a difference between how the trajectory was generated and the model used in the KF. As mentioned in Section 4.4.1.1, the random trajectories were controlled to keep them inside the confines of the hallway. The control action is only applied to the Y-axis portion of the trajectory along the main hallway and the X-axis portion of the trajectory along the side hallway. The random trajectory is generated using the method described in Section 4.4.1.1. After each time step, the distance between the center of the hallway and the new position is compared. The distance between the two is then multiplied by a scale factor and subtracted from the new generated position. The result of this process is that the filter is estimating its uncertainty based on an acceleration uncertainty of .08 meters per second squared, when the actual trajectory, for all simulated runs, is varying less than this. Therefore, the MC runs have shown that the magnetic aided position algorithm can provide positioning solutions within .2 meters (RMS) when the filter has knowledge of the control inputs. In addition to this positioning

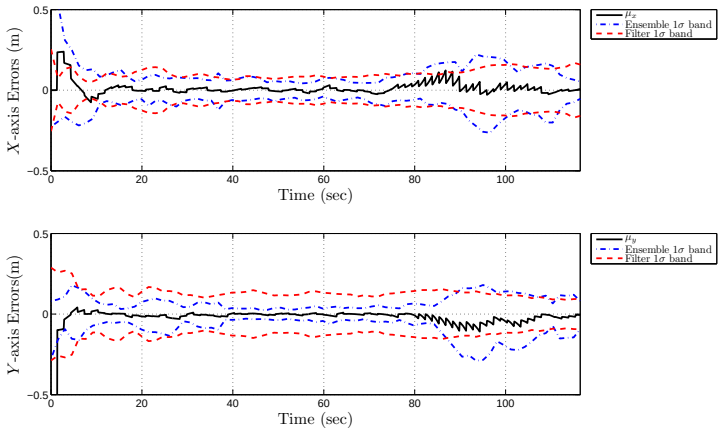

Figure 4.14: Ensemble Statistics: The filter's ability to track the trajectory is contingent on the filter having the correct system model. In this case, the filter model did not include any information about the 90° turn.

accuracy, the MC runs have also shown that the model used in the simulation is correct, with the exception of the control on the trajectory generation. With the MC results understood, the next step is to examine how the algorithm performs when real data is used.

4.4.2 Real Trajectory and Measurements. The second test used the same process and algorithms as the first, but the trajectory was not generated via simulation. Instead, the second test used a real trajectory that took measurements as the cart moved along the pre-described trajectory. There were two different trajectories used to test the algorithm using real measurements. Both trajectories were benign in their variation around the hallway, as the filter's ability to estimate its position, given good measurements, was shown via the MC simulations. The goal of using real measurements was to show that the magnetic field intensity in the indoor environment does vary enough by position, but is stable enough in time to support using a map collected at a previous point in time. The map data used in this portion is the same map data used previously, but the measurements were collected on 5 December 2008.

4.4.2.1 Trajectory Generation. The first trajectory used to demonstrate the use of real measurements is shown in Figure 4.16. To ensure that the tra-

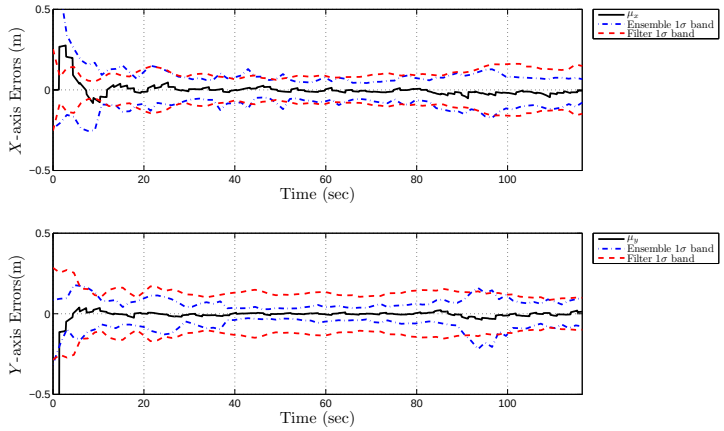

Figure 4.15: Ensemble Statistics: The filter's ability to track the trajectory is contingent on the filter having the correct system model. In this case, the system model is correct and the filter and ensemble statistics match fairly well, which shows the system model is accurate.

jectory used for truth matched the trajectory traveled, the measurements needed to be taken from known locations. The simulation described previously in Section 4.4.1 used a time step of .1 seconds, an update rate of 1.5 sec, and a forward vehicle velocity of .5 meters per second. In order to match this criteria with a real trajectory, a measurement needed to be taken at every second grid point. This was determined by calculating the distance traveled between updates at the nominal velocity, (1.5 seconds $\times$ .5 meters per second), the result of this showed that a measurement needed to be taken every .750 meters. Recall that the grid points were located .381 meters (15 in) apart. The distance between two grid points was .762 meters, which falls within the bounds of the system model.

Using this trajectory, the results, shown in Figure 4.17, show that the real measurements are good enough to keep the vehicle in the hallway, but there are a couple of places where the error exceeds 2 meters. Figure 4.18 shows the measurement residuals of the first trajectory (the residuals, in this case, are found by subtracting the post-update position estimate from the position measurement found using the magnetic aided position algorithm). The locations corresponding to the large position errors are associated with the locations that had large measurement residuals. This

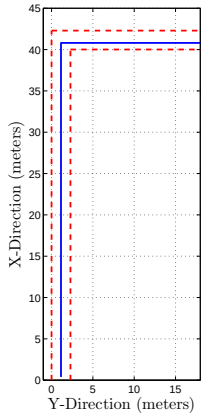

Figure 4.16: Real trajectory near center of hallway. This trajectory was the first trajectory used to demonstrate the performance of the magnetic aided position algorithm using real measurements.

means the magnetic field intensity measurement correlated with a position different from the filter's estimated position by a large margin. Figures 4.4 and 4.6 show that there is not much variation in the middle of the hallway. This lack of variation could lead to the large residuals seen in Figure 4.18.

To help determine if the lack of variation was really the problem, the second trajectory, pictured in Figure 4.19, goes down the right-hand side of the hallway. The same techniques used to generate the trajectory pictured in Figure 4.16 were used to generate this trajectory. The position errors associated with going down the side of the hallway is shown in Figure 4.20. The result is smaller errors and smaller residuals, as shown in Figure 4.21. However, the errors are still significantly larger than the errors generated using the MC simulation.

The trajectory estimation using real measurements was conducted using the same system model as that of the MC simulation. The vehicle was defined as moving at .5$\pm$.08 meters per second. From Figures 4.16 and 4.19, it can be seen that there was virtually no variation in the cross-track direction. This means in the main hallway, there was very little variation in the Y-direction and on the side hallway there was very little variation in the X-direction. Using this observation, the system model was changed to reflect this (σ_a was changed from .08 meters per second squared to .02

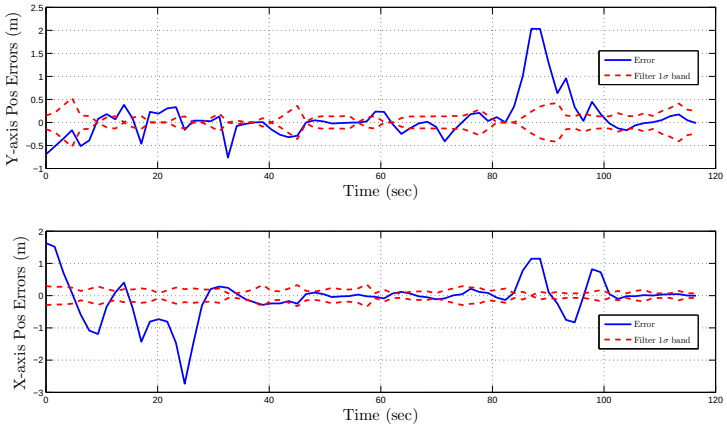

Figure 4.17: Position error plots showing the filter performance using non-simulated measurements from the trajectory shown in Figure 4.16.

meters per second per squared). Figures 4.22 and 4.23 show the improved results for the trajectory down the middle of the hallway and the trajectory down the side of the hallway, respectively. The position error for the first real trajectory went from having a maximum position error of over two meters to having a position error of a meter or less. The second trajectories performance improved just as dramatically. Originally it had a maximum error of approximately 1.5 meters, and now the maximum error for that trajectory is .6 meters. This illustrates the importance of having the correct system model in the KF.

4.5 Leader-Follower Algorithm Implementation

The leader-follower algorithm is a relative positioning algorithm that uses magnetic field data, measured by the leader, to aid the position estimate of a follower. The follower then uses this position estimate to control its path to remain close to the path of the lead vehicle. The implementation as designed in Section 3.5 would not work for a σ_a of .08 meters per second squared. The reason for this is that the second vehicle must follow the trajectory of the first vehicle reasonably well, or the second vehicle will not remain inside the span of the leader's measurements. If the follower is outside of the span of the leader's measurements, the follower will not be able to

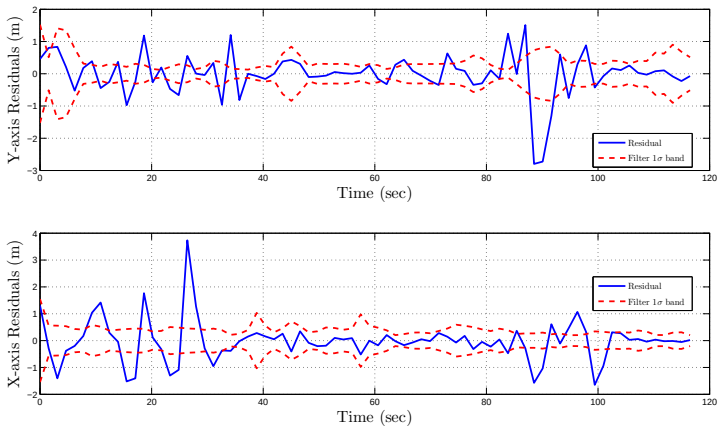

Figure 4.18: Measurement residuals of the first non-simulated trajectory. The large position errors in Figure 4.17 correspond to a bad measurement value. These can be attributed to areas with little magnetic variation.

estimate its position. After simulating the leader-follower algorithm using different values for σ_a, the largest value successfully implemented was .02 meters per second squared, which was used in both the lead vehicle's system model and the follower vehicle's system model.

4.5.1 Leader-Follower Performance Analysis. With the lead vehicle trajectory constant and magnetic measurements taken along this trajectory with three sensors, the follower tracking ability was tested using 50 simulation runs and a σ_a of .02 meters per second squared. Out of the 50 runs, zero were completed or successful. A completed run is defined as a run where the follower makes it at least 16 meters down the side hallway. A successful run, for this implementation, is defined as a run that tracks the leader at least 10 meters down the side hallway, which is 55 percent of the side hallway length and approximately 90 percent of the total path. The reason for the 10 meter threshold is there is a section of the side hallway (right around 10 meters) that does not have a lot of variation. As mentioned in Section 4.2.1, if an area does not have large variations, the magnetic aided position algorithm will not accurately determine its position. For the current leader-follower implementation, this problem is magnified, because the follower vehicle is trying to ascertain where it

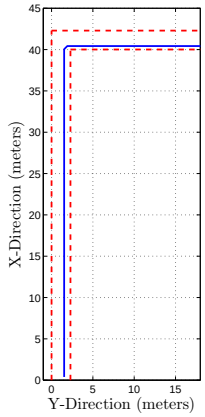

Figure 4.19: Real trajectory near right side of hallway. This trajectory was the second trajectory used to demonstrate the performance of the magnetic aided position algorithm using real measurements. This trajectory takes advantage of the large variations present near structures such as walls and floors.

is with respect to the leader's estimated trajectory. If the follower picks the wrong location, the control input could command the follower in the wrong direction.

For example, if the position estimate generated by the follower vehicle is to the right of the leader's estimated trajectory, but the follower vehicle is actually to the left of the leader's estimated trajectory, then the control input generated by the magnetic aided position algorithm will command the follower vehicle to go further to the left, which will take the follower vehicle further from the reference trajectory. If there is enough variation in the magnetic field at this commanded position, the magnetic aided position algorithm will realize the follower is to the left of the reference trajectory with the next estimate and correct its position accordingly. If there is not enough variation, then the magnetic aided position algorithm could estimate the vehicle's position as being to the right of the reference trajectory again and command the vehicle further to the right. This phenomenon was the cause of all unfinished runs in the lead-follower implementation. Figure 4.24 shows one case of this phenomenon.

To avoid the phenomenon created by the lack of large variations, two different approaches were implemented. The first implementation was a fix to the algorithm that moves the actual vehicle back to the center of the hallway. This method, as

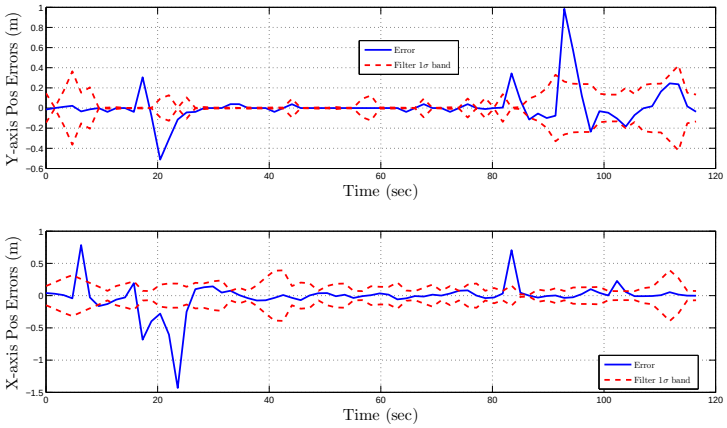

Figure 4.20: Position error plots showing the filter performance using the non-simulated measurements from the trajectory shown in Figure 4.19.

implemented, is primarily a tool to show that the algorithm would function properly if the vehicle managed to move back to the path of the lead vehicle (perhaps by turning away from walls). In the simulation, this was done by monitoring the vehicle's actual position in the hallway. If the vehicle reached a point where it would be physically outside the confines of the hallway, much like the case of the generated trajectory in Section 4.4.1, then the vehicle's position would be reset to the opposite side of the center of the hallway. This implementation improved the performance, but did not eliminate the failure mode. The number of successful runs out of 50 using this approach went from 0 to 18 and the number completed went from 0 to 2.

The second approach used an additional sensor in the lead vehicle. The goal of this approach was to show that the addition of a fourth sensor would widen the sensed magnetic field by the leader, allowing for the follower to be farther from the leader's trajectory, but still have valid magnetic field measurements. This method improved the performance over the three sensor case, with and without the position reset. Out of 50 runs using this approach, 9 were completed and 18 were successful in tracking the leader for over 90 percent of the total trajectory.

To increase the successful tracking percentage, the second approach was combined with the first approach. By adding a fourth sensor and resetting the vehicle's

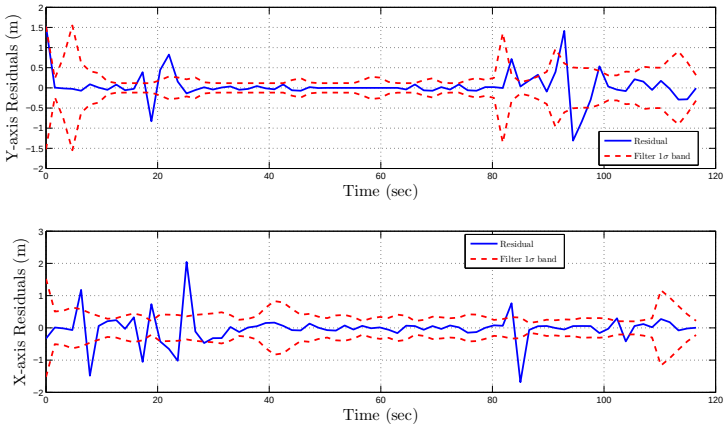

Figure 4.21: Measurement residuals of the second non-simulated trajectory. The large position errors in Figure 4.20 are not as large as those in Figure 4.17. This is due to greater magnetic field variation along the side of the hallway, which equate to more accurate position measurements.

position if the vehicle "hit" a wall, the number of successful runs was 36 and the number of completed runs was 23. Table 4.2 shows the different levels of performance achieved by each implementation. As expected, adding more sensors and having some way of monitoring the validity of a position estimate (i.e., residual monitoring, likelihood thresholding, etc.) has the highest level of success.

4.5.2 Leader-Follower Estimation Error. As mentioned in previous sections, the goal of the leader-follower algorithm is to have the follower track the trajectory of the leader. However, since the lead vehicle only has an estimate of its true trajectory (this is the reference trajectory passed to the follower), the follower can only track the estimated trajectory of the leader. Therefore, the position estimate generated by the follower is in the wrong reference frame to compare it to the leader's true trajectory. The goal of the leader-follower algorithm is to show how well the follower follows the path of the leader. In order to do this, the leader's estimated trajectory must be resolved in the reference frame of leader's actual trajectory. Once this transformation is executed, the follower's position can be determined with respect to the leader's position. The difference in reference frame means that each position measurement

Table 4.1: Parameter values used for the simulations that demonstrate the magnetically aided INS.

Parameter	Value
Time Step Δt	0.1 sec
Initial X-Direction Velocity (V_X)	.5 m/s
Initial Y-Direction Velocity (V_Y)	0 m/s
Initial Filter X-Position (P_X)	0 m
Initial Filter Y-Position (P_Y)	0 m
Initial Vehicle X-Position (P_X)	0 m
Initial Vehicle Y-Position (P_Y)	1.145 m
Initial X-Position Uncertainty (σ_{P_X})	1.5 m
Initial Y-Position Uncertainty (σ_{P_Y})	1.5 m
Acceleration Uncertainty Both Axes (σ_a)	.08 m/s^2
Magnetometer Measurement Noise (σ_{meas})	1 $milli - gauss$
Filter Update Interval	1.5 sec

Table 4.2: Performance comparison of the leader-follower algorithm, using different techniques to aid the magnetic aided position algorithm in areas of small variations. The number of completed runs are the runs where the follower made it at least 16 meters down the side hallway, whereas a successful run was considered runs that made it to 10 meters, the successful run column includes the completed runs.

Implementation	Number of Complete Runs	Number of Successful Runs	Number Past Turn	Number Not Making Turn
Three Sensors No Pos. Reset	0 (0%)	0 (0%)	0 (0%)	50 (100%)
Three Sensors Pos. Reset	2 (4%)	18 (36%)	33 (66%)	17 (34%)
Four Sensors No Pos. Reset	9 (18%)	18 (36%)	38 (76%)	12 (24%)
Four Sensors Pos. Reset	23 (46%)	36 (72%)	41 (82%)	9 (18%)

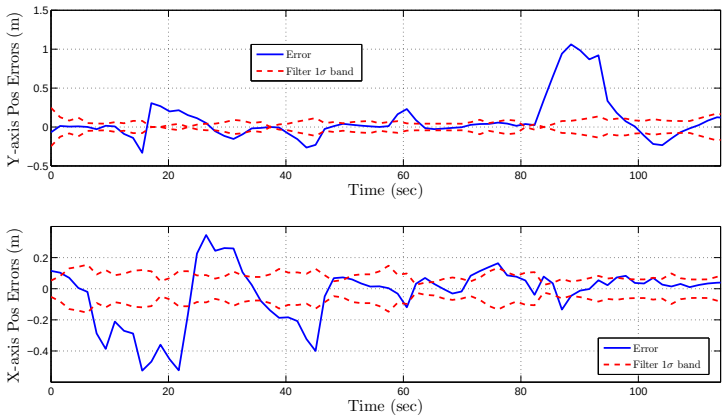

Figure 4.22: Position error plots showing the filter performance using the non-simulated measurements from the trajectory shown in Figure 4.16 and $\sigma_a = .02\ m/s^2$.

generated by the magnetic aided position algorithm is offset by the difference between the leader's true trajectory and the leader's estimated trajectory. The error between the follower's position estimate and the leader's position estimate is calculated for use in the PID controller as described in Section 3.5.2. However, to view the follower's trajectory with respect to the leader's true trajectory the follower's actual position must be transformed into the leader's reference frame. The process used to complete this transformation can be viewed in Appendix A.

The follower's true trajectory is plotted with the leader's estimated trajectory in Figure 4.25a. However, as mentioned previously, the result in Figure 4.25a does not show how well the follower tracked the leader. Figure 4.25b shows the corrected follower trajectory. The case shown is for a leader trajectory that veers to the right of the reference trajectory along the main hallway and then veers to the left on the side hallway. There is a gap in the follower's trajectory as the actual trajectory crosses over the reference trajectory in Figure 4.25. This is a result of the calculation used to transform the follower's trajectory into the leader's reference frame. If the two vehicle's were actually observed through this process, there would be no break in the data. The data presented here is from the four sensor implementation, with and without the position reset.

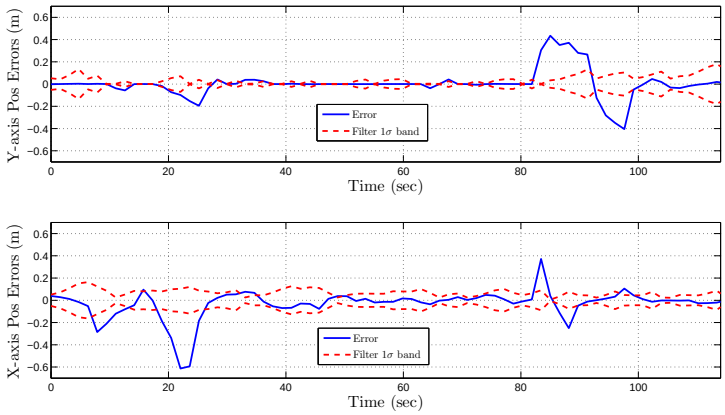

Figure 4.23: Position error plots showing the filter performance using the non-simulated measurements from the trajectory shown in Figure 4.19 and $\sigma_a = .02\ m/s^2$.

To further illustrate the leader-follower implementation, Figure 4.26 shows the same information as Figure 4.25, but for a true trajectory that veers to the left along the main hallway. Notice the sawtooth-like variation in the follower's trajectory. This is introduced by the position reset routine described in Section 4.5.1. The two figures just presented demonstrate that the transformation works for almost all situations. The only error in this process comes from a singularity when the two leader's trajectories cross one another.

Now that the trajectories are in the correct frame of reference, the actual errors between the leader's true trajectory and the follower's true trajectory can be calculated. The errors presented in Figures 4.27 and 4.28 were calculated by subtracting the leader's true value from the follower's true value. Recall that the goal of the control action was to minimize the cross-track error between the follower's actual trajectory and the leader's actual trajectory. Using the transformation shown in Appendix A, the cross-track errors are shown to be less than .4 meters. These results are typical of the cases that completed a successful run.

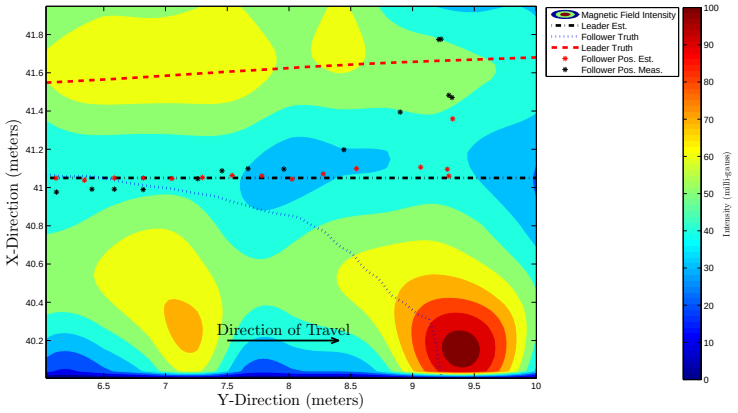

Figure 4.24: Example of the failure mode induced by small magnetic variations. Notice the position measurement and estimate are on the opposite side of the reference trajectory. The tracking command, u_2, commands the vehicle to turn away from the reference trajectory.

4.6 Summary

This chapter demonstrated that the magnetic aided position algorithm can provide position solutions with sub-meter level accuracy. Using a map of an entire area to estimate a random trajectory produced RMS errors of less than .3 meters, while the leader-follower algorithm produced errors less than .4 meters, as long as the follower stayed within the range of measurements provided by the leader.

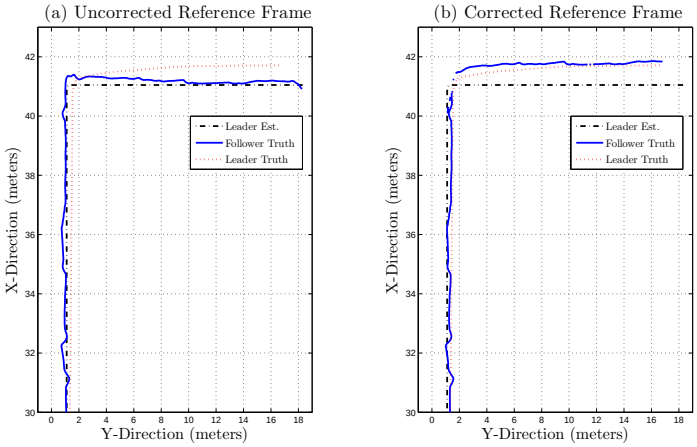

Figure 4.25: The follower's trajectory shown in both reference frames. (a) Shows the follower's trajectory in the leader's estimated trajectory reference frame and (b) shows the follower's reference frame resolved in the leader's true trajectory frame. The leader's true trajectory, in this case, veered to the right along the main hallway and to the left on the side hallway.

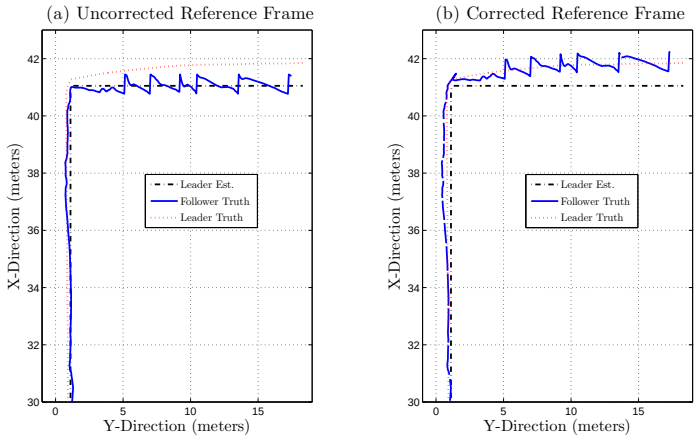

Figure 4.26: The follower's trajectory shown in both reference frames. (a) Shows the follower's trajectory in the leader's estimated trajectory reference frame and (b) shows the follower's reference frame resolved in the leader's true trajectory frame. The leader's true trajectory, in this case, veered to the left along the main hallway and to the left on the side hallway. The sawtooth variations along the side hallway are due to the position reset algorithm.

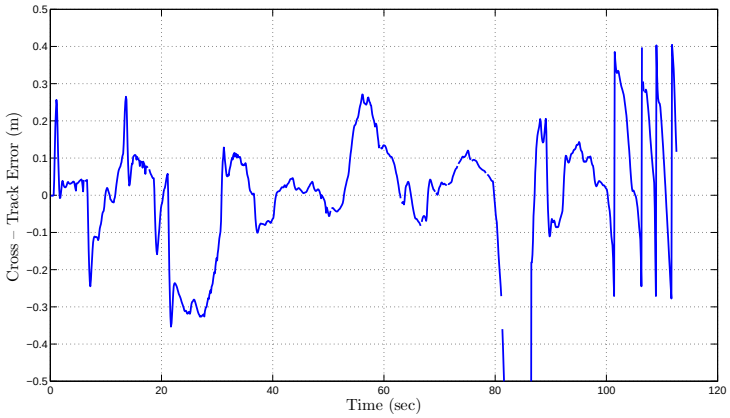

Figure 4.27: The position errors between the follower trajectory and the leader trajectory. The rise in error following the turn at 80 seconds is caused by no control along the path of travel. This case used the position reset algorithm.

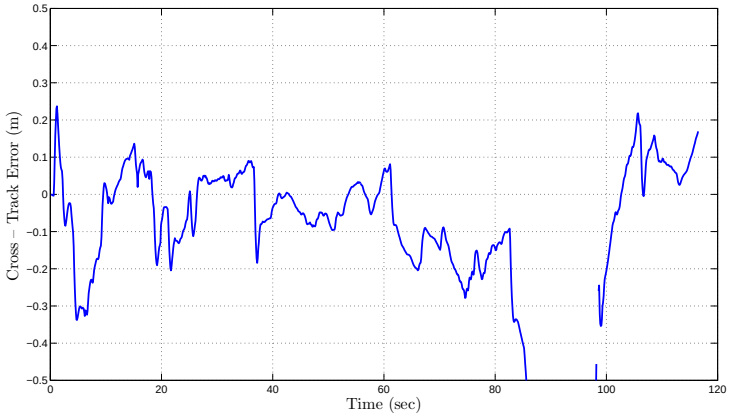

Figure 4.28: The position errors between the follower trajectory and the leader trajectory. The rise in error following the turn at 80 seconds is caused by no control along the path of travel. This case did not use the position reset algorithm.

V. Conclusions and Recommendations

THIS research has demonstrated the feasibility of using magnetic field variations to aid inertial navigation systems. The method demonstrated modified a multi-beam terrain navigation approach to take advantage of the three distinct measurements provided by the three-axis magnetometers. The adapted approach uses a KF and a magnetic aided position algorithm to aid the inertial system. The magnetic aided position algorithm relates the magnetic field intensity measurements to a specific position through the use of a map of magnetic field intensities for each of the three magnetometer axes. The maps were generated using magnetic field intensity data collected at equally spaced grid points and then interpolated to provide closer grid spacing.

5.1 The Magnetic Aided Position Algorithm

Following the generation of the magnetic field intensity maps, the position measurement update was generated using the magnetic aided position algorithm. The magnetic aided position algorithm calculates the position measurement by applying Bayes' rule to the results of a maximum likelihood function and the propagated pdf generated via the KF. The measurement update was then incorporated with the KF position estimate with the standard KF update equations. The positon aiding algorithm, as developed, was applied in three different cases: a MC simulation with simulated measurements generated from the magnetic field map, a test using real measurements, and a leader-follower simulation.

5.2 Magnetic Aided Position Algorithm Tests

The MC simulation showed that the inertial system, with aiding provided by the magnetic aided position algorithm, was able to successfully track 100 random trajectories with RMS errors of less than .3 meters.

The test of the magnetic aided position algorithm using real measurements helped to verify that the process used for the MC simulation was valid, as well as

to illustrate that indoor magnetic field intensities are stable enough to be mapped, stored, and used at a later date for position sub-meter position solutions.

The leader-follower algorithm demonstrated one application of this magnetic aided position algorithm. The leader collects magnetic field intensity data as it moves through an area and then passes this information to a second vehicle. The follower then uses the magnetic data, the estimated trajectory, and any turn commands from the leader to track the lead vehicle through an environment. The leader-follower implementation requires both the leader and follower to have more accurate speed control ($\sigma_a = .02\ m/s^2$) than when the position aided algorithm is implemented using the map of an entire area ($\sigma_a = .08\ m/s^2$). The need for less variation on the acceleration of the leader and follower is because the map generated with this approach is a subset of the entire area. If the follower gets outside the bands of the magnetic map generated by the leader, there is no information available to aid the follower.

Initially, the leader-follower algorithm used three sensors on the leader to measure the magnetic field. Upon implementation, three sensors were found to be inadequate to meet performance goals. The three sensor approach makes the magnetic aided position algorithm more susceptible to, in terrain navigation terminology, "flat-bottomed" areas, which are areas where the magnetic variation between points is less than the measurement noise of the magnetometers. To overcome this in simulation, a position reset algorithm was implemented. In addition to the problem of "flat-bottomed" areas, the three sensors did not provide enough map coverage to achieve the desired performance goals. Therefore, an additional sensor was added to the leader. By adding the fourth sensor and the position reset algorithm, performance was increased dramatically. Using this method resulted in the follower tracking the leader within .4 meters.

5.3 The Way Ahead

While this research has shown the potential of using magnetic field intensity information to aid indoor position information, there are still several aspects that should be considered. Among these are the length of time magnetic intensity values are valid, the benefits of using heading reference information, ways to improve performance of the leader-follower algorithm, and how to overcome the "flat-bottomed" areas.

The length of time between the collection of the magnetic map data and the real measurements was two weeks. Throughout the literature, there has not been much characterization of magnetic field variations in an indoor environment, except to say that the variations prevent electronic compasses from working properly [13]. While this research shows the variations to be stable enough for success over a two week time period, it is necessary to know when the measurements no longer become valid. A possible solution to the time stability question would be to subtract out the Earth's changing field and compare just the magnetic anomalies present in the indoor environment. This is the method used in [19] for the outdoor case.

For simplification purposes, vehicle heading information was not directly used in this research. Magnetic field intensity is a three dimensional vector at any given point. This vector is described by the three-axis measurements provided by the magnetometers. If the magnetic intensity is collected at a known location and orientation, the heading of a vehicle can be determined by finding the point of maximum likelihood using the total magnitude of the magnetic field intensity and then finding the orientation that matches the three-axis measurement. The heading information would allow for a more accurate control of the vehicle as it moves through an environment and provide more precise positioning information. However, from a computational standpoint, it would require searching over one more dimension (x,y position plus heading, as opposed to x,y position).

A couple of methods already investigated for improving the performance of the leader-follower implementation were adding an additional sensor to the leader and implementing a position reset algorithm in the second vehicle. In the simulation, the position was reset by detecting when the vehicle hit the "wall" of the hallway. This can be implemented on a real vehicle by using a touch sensor on each side of the vehicle. If the right touch sensor is activated, the vehicle could be controlled to the left a prescribed distance and then the magnetic aided position algorithm could take over control. This method treats the symptom of the problem as opposed to the problem itself, which is a lack of variation in the magnetic field.

Adding an additional sensor on the leader helped reduce the problems caused by a lack of variation, but did not eliminate them. Another approach would be to add an additional sensor to the follower. The second sensor would allow at least two different methods to be used to remove the ambiguity seen in the "flat-bottomed" areas. The first method would be to combine the measurements from the second sensor with the measurements from the first sensor in the likelihood function to help remove the ambiguity. This approach comes from the observation in [11] that more measurements help to remove erroneous measurements. The second method would be to find the position of each magnetometer using the likelihood function and then combine that information with the geometry of the sensor array. If the positions found using the likelihood function are not feasible due to the physical layout of the system, then these position updates could be ignored, or the results of the likelihood function could be compared to find the points that do match the physical layout of the sensor array.

Overall, the processes developed and implemented for this research show that magnetic field intensity can be used as a viable source of position data indoors. While areas of limited magnetic variation pose the largest problem for this navigation approach, the problems could be overcome by using some of the above approaches or by combining this approach with other indoor navigation techniques, such as vision-aided navigation.

Appendix A. Leader-Follower Coordinate Transformation

FIGURE A.1 is a graphical representation of the error transformation, with $\mathbf{x_{r1/2}}$ representing the position estimate of the leader, $\mathbf{x_{actual1/2}}$ representing the actual trajectory of the lead vehicle, and $\mathbf{x_{plant}}$ representing the follower's position at a given instant in time. The subscript 1/2 represent the two closest positions to $\mathbf{x_{plant}}$ from the respective trajectories. With Figure A.1 as a reference, the point C is found using the procedure outlined in Section 3.5.2, with the position estimate, $\mathbf{x}(t_k^+)$, replaced by $\mathbf{x_{plant}}$. The next step is to determine the distance between C and B'. Since $\mathbf{x_{actual}}$ and $\mathbf{x_r}$ are discrete, B' may be between discrete points and cannot be found directly. Therefore, the Law of Sines can be used to find the length B.

In order to use the Law of Sines, which states

$$\frac{A}{\sin(A)} = \frac{B}{\sin(B)} = \frac{C}{\sin(C)}, \tag{A.1}$$

at least two sides and an angle or two angles and one side must be known. In this case, the length of A, the length of D, and the angle between A and B can be found from the known information. The length of A is calculated by finding the norm of $\vec{A}$, which is the vector that points from point C to point $\mathbf{x_{actual1}}$. If there exists two vectors, the angle between them can be calculated. The vector between C and B' is not known, but the unit vector between C and B' is known, it is equal to the unit vector of Δp, $\vec{u}_{\Delta p}$. Therefore, the angle between $\vec{A}$ and $\vec{u}_{\Delta p}$, is found using

$$\delta = cos^{-1}\left(\frac{\vec{A}\cdot\vec{u}_{\Delta p}}{||\vec{A}||||\vec{u}_{\Delta p}||}\right). \tag{A.2}$$

With δ and A known, the next step is to find the angle opposite side A, α. The angle α is found by calculating the angle between $\vec{u}_{\Delta p}$ and $\vec{u}_D$, which is the unit vector of the vector that extends from $\mathbf{x_{actual2}}$ to $\mathbf{x_{actual1}}$, and subtracting that angle from 180°. Using Equation A.1 and the values calculated for A, α, and δ, the length of D is calculated. The length of D is added to $\mathbf{x_{actual1}}$ to determine the location of B'.

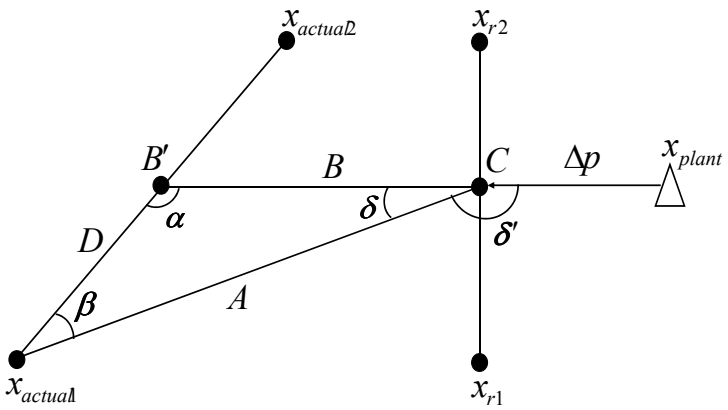

Figure A.1: The geometric representation used to determine the calculations needed to convert the follower's trajectory into the leader's true trajectory frame of reference.

The vector $\vec{B}$ is then calculated by subtracting B' from C. With $\vec{B}$, the error vector is calculated by multiplying the norm of $\vec{B}$ times $\vec{u}_{\Delta p}$.

If $\mathbf{x_{plant}}$ is located between the leader's true trajectory and the leader's estimated trajectory, $\vec{u}_{\Delta p}$ will point in the direction opposite of the actual error. This creates a situation where δ is calculated as δ'. Therefore, if the value calculated for δ is greater than 90°, δ is subtracted from 180° and the sign of $\vec{u}_{\Delta p}$ is reversed.

Bibliography

1. Campbell, Wallace Hall. *Earth Magnetism: A Guided Tour through Magnetic Fields*. Complementary Science Series. Harcourt/Academic Press, San Diego, CA, 2001.

2. Fraden, Jacob. *Velocity and Acceleration*, 301–312. Handbook of Modern Sensors - Physics, Designs and Applications. Springer Science Business Media, LLC, 233 Spring Street, New York, New York, 10013, USA, 3rd edition, 2000. Http://www.knovel.com/knovel2/Toc.jsp?BookID=1698&VerticalID=0.

3. Goldenberg, Advanced Sensors Technical Center), Felix (Goodrich Corporation. "Geomagnetic navigation beyond the magnetic compass". *Record - IEEE PLANS, Position Location and Navigation Symposium, IEEE/ION Position, Location, and Navigation Symposium*, 2006:684–694, 2006.

4. Honeywell, Solid State Electronics Center. "HMR2300 Smart Digital Magnetometer Datasheet". `http://www.ssec.honeywell.com/magnetic/datasheets/hmr2300.pdf`.

5. Leon-Garcia, Alberto. *Probablity and random processes for electrical engineers*. Addison-Wesley Publishing Company, Inc., Reading, MA, 2 edition, May 1994.

6. Lohmann, Kenneth J., Catherine M. F. Lohmann, and Nathan F. Putman. "Magnetic maps in animals: nature's GPS". *The Journal of Experimental Biology*, 210(21):3697–3705, November 2007.

7. Maybeck, Peter S. *Stochastic Models, Estimation, and Control*, volume 2. Academic Press, INC., New York, New York, 1982.

8. Maybeck, Peter S. *Stochastic Models, Estimation, and Control*, volume 1. Navtech Book and Software Store, Arlington, VA, 1994.

9. Misra, Pratap and Per Enge. *Global Positioning System: Signals, Measurements, and Performance*. Ganga-Jamuna Press, Lincoln, MA, second edition, 2006.

10. Nelson, James H., Loius Hurwitz, and David G. Knapp. *Magnetism of the Earth*. Publication 40-1, United States Department of Commerce: Coast and Geodetic Survey, Washington D.C., 1962.

11. Nygren, I. "Robust and efficient terrain navigation of underwater vehicles", 2008. ID: 1.

12. Ogata, Katsuhiko. *Modern Control Engineering*. Prentice Hall, Upper Saddle River, NJ, 4 edition, 2002.

13. Skvortzov, Vladimir Y., Hyoung-Ki Lee, SeokWon Bang, and YongBeom Lee. "Application of Electronic Compass for Mobile Robot in an Indoor Environment".

International Conference on Robotics and Automation, 2963–2970. Institute of Electrical and Electronics Engineers, Rome, Italy, April 2007.

14. Strangway, David W. *History of the Earth's Magnetic Field*. McGraw-Hill, Inc., New York, NY, 1970.

15. Support, MIDG II. "MIDG II Magnetometer Data". Email, October 2008. This was an email from MIDG II technical support regarding units of magnetometer data.

16. Titterton, David H. and John L. Weston. *Strapdown Inertial Navigation Technology*. The Institution of Electrical Engineers, Michael Faraday House, Six Hills Way, Stevenage, Herts. SG1 2AY, United Kingdom, 2004.

17. Veth, Michael J. *Fusion and Imaging Sensors for Navigation*. Ph.D. thesis, Air Force Institute of Technology, 2006.

18. Veth, Mike and John Raquet. "Inertial Sensor Modeling", September 2005. AFIT EENG 699 Course Notes.

19. Wilson, John M., Robert J. Kline-Schoder, Marc A. Kenton, Paul H. Sorensen, and Odile H. Clavier. "Passive Navigation Using Local Magnetic Field Variations". *Institute of Navigation International Technical Meeting*, 770–779. Institute of Navigation, Monterey, CA, January 2006.

REPORT DOCUMENTATION PAGE

Form Approved
OMB No. 0704–0188

1. REPORT DATE *(DD–MM–YYYY)*	2. REPORT TYPE	3. DATES COVERED *(From — To)*
26–03–2009	Master's Thesis	Aug 2007 — Mar 2009

4. TITLE AND SUBTITLE

Magnetic Field Aided Indoor Navigation

5a. CONTRACT NUMBER

5b. GRANT NUMBER

5c. PROGRAM ELEMENT NUMBER

6. AUTHOR(S)

William F. Storms, Capt, USAF

5d. PROJECT NUMBER

ENG 09-224

5e. TASK NUMBER

5f. WORK UNIT NUMBER

7. PERFORMING ORGANIZATION NAME(S) AND ADDRESS(ES)

Air Force Institute of Technology
Graduate School of Engineering and Management (AFIT/EN)
2950 Hobson Way
WPAFB OH 45433-7765

8. PERFORMING ORGANIZATION REPORT NUMBER

AFIT/GE/ENG/09-44

9. SPONSORING / MONITORING AGENCY NAME(S) AND ADDRESS(ES)

Air Force Research Laboratory, Munitions Directorate
Advanced Guidance Division (Dr. Mikel M. Miller)
101 West Eglin Blvd, Building 13
Eglin Air Force Base, FL 32542
(850-882-4033, mikel.miller@eglin.af.mil)

10. SPONSOR/MONITOR'S ACRONYM(S)

AFRL/RWG

11. SPONSOR/MONITOR'S REPORT NUMBER(S)

12. DISTRIBUTION / AVAILABILITY STATEMENT

Approval for public release; distribution is unlimited.

13. SUPPLEMENTARY NOTES

14. ABSTRACT

Many current aiding methods do not work well in an indoor environment, like aiding using the Global Positioning System. The method presented in this research uses magnetic field intensity data from a three-axis magnetometer in order to estimate position using a maximum – likelihood approach. The position measurements are then combined with a motion model using a Kalman filter. The magnetic field navigation algorithm is tested using a combination of simulated and real measurements. The result of these tests show that the position aiding algorithm is capable of generating positon estimates from real data within less than 1 meter of the true trajectory, with most estimates .3 meters away from the true trajectory in a laboratory hallway environment. To further explore the capabilities of the position aiding algorithm, a leader-follower scenario is implemented. In this scenario, the follower uses magnetic field intensity data collected by the leader to estimate its current position and attempt to follow the leader's trajectory. The results show that tracking is possible, and that the measurement span of the leader has a large impact on the result.

15. SUBJECT TERMS

indoor navigation, magnetic field navigation, kalman filter aided navigation, sub-meter positioning solutions

16. SECURITY CLASSIFICATION OF:			17. LIMITATION OF ABSTRACT	18. NUMBER OF PAGES	19a. NAME OF RESPONSIBLE PERSON
a. REPORT	b. ABSTRACT	c. THIS PAGE			Dr. John F. Raquet
U	U	U	UU	86	19b. TELEPHONE NUMBER *(include area code)* (937) 255–3636, ext 4580; john.raquet afit.edu